Structures of NF-κB p52 homodimer-DNA complexes rationalize binding mechanisms and transcription activation

Vladimir A. Meshcheryakov[1,6,7], Wenfei Pan[1,6], Tianjie Li[2], Yi Wang[2], Gourisankar Ghosh[3], and Vivien Ya-Fan Wang[1,4,5,*]

[1]Faculty of Health Sciences, University of Macau, Avenida da Universidade, Taipa, Macau SAR, China
[2]Department of Physics, The Chinese University of Hong Kong, Shatin, NT, Hong Kong SAR, China
[3]Department of Chemistry and Biochemistry, University of California, San Diego, 9500 Gilman Drive, La Jolla, CA 92093, USA
[4]Cancer Centre, Faculty of Health Sciences, University of Macau, Avenida da Universidade, Taipa, Macau SAR, China
[5]MoE Frontiers Science Center for Precision Oncology, University of Macau, Avenida da Universidade, Taipa, Macau SAR, China
[6]These authors contributed equally
[7]Present address: Molecular Cryo-Electron Microscopy Unit, Okinawa Institute of Science and Technology Graduated University, Onna, Kunigami, Okinawa, Japan

* To whom correspondence should be addressed. Email: vivienwang@um.edu.mo

Keywords: DNA conformation, NF-κB, crystal structure, MD simulation, thermodynamics, kinetics, transcriptional regulation

Abstract

The mammalian NF-κB p52:p52 homodimer together with its cofactor Bcl3 activates transcription of κB sites with a central G/C base pair (bp), while it is inactive toward κB sites with a central A/T bp. To understand the molecular basis for this unique property of p52, we have determined its structure in complex with a P-selectin(PSel)-κB DNA (5'-GGGGTGACCCC-3') (central bp is underlined) and variants changing the central bp to A/T or swapping the flanking bp. The structures reveal a nearly two-fold widened minor groove in the central region of the DNA as compared to all other currently available NF-κB-DNA complex structures, which have a central A/T bp. Molecular dynamics (MD) simulations show free DNAs exist in distinct preferred conformations, and p52:p52 homodimer induces the least amount of conformational changes on the more transcriptionally active natural PSel-κB DNA in the bound form. Our binding assays further demonstrate that the fast kinetics driven by entropy is correlated with higher transcriptional activity. Overall, our studies have revealed a novel conformation for κB DNA in complex with NF-κB and suggest the importance of binding kinetics, dictated by free DNA conformational and dynamic states, in controlling transcriptional activation for NF-κB.

Introduction

The binding of transcription factors (TFs) to their specific DNA response elements in the promoters/enhancers of target genes is the key event regulating gene transcription and consequent cellular processes. For proper gene expression, TFs must interact selectively at the correct place and time and assemble into high-order complexes with specific DNA sequences and cofactors (Natoli et al., 2005, Mulero et al., 2019). In eukaryotic genomes, the ability of TFs to select a small subset of relevant binding sites out of the large excess of potential binding sites within the genomes is the foundation upon which transcriptional regulation is built. Structural studies have provided valuable information on how various DNA binding domains recognize their cognate DNA binding sites at atomic resolution (Garvie and Wolberger, 2001). However, how TFs discriminate between closely related, but biologically distinct, DNA sequences is not well understood.

The NF-κB family of TFs regulates diverse biological responses (Zhang et al., 2017). Mammalian NF-κB is assembled combinatorially from five subunits, p50/NF-κB1, p52/NF-κB2, RelA/p65, c-Rel and RelB, into homo- and heterodimers which bind to specific DNA sequences, known as κB site or κB DNA. All five subunits share a highly conserved region at their N-termini, referred to as the Rel homology region (RHR), and the three-dimensional structures of the RHR are also highly conserved among these proteins. The RHR is roughly 300 residues in length and contains the N-terminal domain (NTD), dimerization domain (DD) and nuclear localization signal (NLS). The DD alone mediates protein homo- and heterodimerization; the NTD and DD together are responsible for DNA binding; the NLS region is flexible in solution and together with the DD forms the binding sites for the inhibitor of NF-κB (IκB) proteins.

The NF-κB proteins can be further divided into two sub-classes: the p50 and p52 subunits belong to class I by virtue of their lack of a transcriptional activation domain (TAD). The other three subunits, RelA, c-Rel and RelB, constitute class II with every member containing a TAD at its C-terminus. Mature p50 and p52 subunits are generated via incomplete proteolysis of their precursor proteins p105 and p100 (Supplemental Fig. S1A), respectively. Therefore, p50 and p52 possess a short glycine rich region (GRR) at their C-termini.

The initial discovery and characterization of several physiological κB DNAs established the pseudo-symmetric consensus sequence as 5'-(–5)G(–4)G(–3)G(–2)R(–1)N(0)W(+1)Y(+2)Y(+3)C(+4)C-3' (Lenardo and Baltimore,

1989), where R = purines, N = any nucleotides, W = either A or T, and Y = pyrimidines. The subsequent identification of new NF-κB-DNA binding sites broadened the consensus to 5'-(–5)G(–4)G(–3)G(–2)N(–1)N(0)N(+1)N(+2)N(+3)C(+4)C-3' (Chen and Ghosh, 1999, Mulero et al., 2019). The critical features of the consensus κB DNA sequence are the presence of a series of G and C bases at the 5' and 3' ends, respectively, while the bases at the central region can vary. X-ray structures of various NF-κB dimers in complex with different κB DNAs revealed conserved protein-DNA recognition modes for κB DNA that follows the consensus sequence (Muller et al., 1995, Ghosh et al., 1995, Cramer et al., 1997, Chen et al., 1998a, Huang et al., 2001, Moorthy et al., 2007, Fusco et al., 2009, Chen et al., 1998b, Chen et al., 2000, Escalante et al., 2002, Berkowitz et al., 2002, Chen-Park et al., 2002, Panne et al., 2007). The RHR of each monomer binds to half of a κB DNA, called half-site. A set of conserved amino acid (aa) residues mediate base-specific contacts to the 5' and 3' flanking G and C bases; the inner, more variable bases participate in important, but less base-specific interactions. The central bp lies at the pseudo-dyad axis of the dimer and is not directly contacted by the protein.

Genome-wide NF-κB-DNA motif identification studies revealed that NF-κB associates not only with consensus κB DNAs, but also with sequences containing only one half-site consensus, and even some sequences with no consensus (Lim et al., 2007, Martone et al., 2003, Zhao et al., 2014). *In vitro* binding experiments have been carried out to classify κB DNAs according to their binding specificity for different NF-κB dimers. The binding affinity displayed by various NF-κB dimers for distinct κB DNAs does not necessarily correlate with what occurs during regulation of gene expression *in vivo*. For example, the p50:RelA heterodimer binds tightly to most κB DNAs, whereas RelA:RelA and c-Rel:c-Rel homodimers bind many of the same sequences with relatively low affinity. However, detailed genetic experiments have shown that some genes are activated only in the presence of one or a subset of NF-κB subunits, such as mice lacking c-Rel exhibit defects in IL-2 and IL-12 expression (Kontgen et al., 1995, Hoffmann et al., 2003). In addition to specific gene activation, NF-κB dimers are also known to repress transcription. The RelA and p50 dimers have been shown to repress the expressions of *nrp1* gene, which is essential for osteoclast differentiation, and the interferon-stimulated response element (ISRE), respectively (Cheng et al., 2011, Hayashi et al., 2012). Both of these sites also display only half-site similarity to the κB DNA consensus. Structural and biochemical analyses of NF-κB-DNA binding have also

revealed the existence of a large number of κB DNAs that display relatively similar affinities compared with κB consensus even though they lack one consensus half-site entirely (Ghosh et al., 2012, Siggers et al., 2011). Therefore, *in vitro* data do not fully capture the complexity of DNA recognition and gene regulation by NF-κB in cells.

NF-κB p52 is generated from the precursor protein p100 (Supplemental Fig. S1A), a tightly regulated process that requires specific stimuli. Unregulated p100 processing into p52 results in multiple myeloma and other lymphoid malignancies, which is detrimental to normal cellular function (Courtois and Gilmore, 2006, Annunziata et al., 2007, Keats et al., 2007). We previously demonstrated that the p52:p52 homodimer could sense a single bp change from G/C to A/T at the central position of a κB DNA (Wang et al., 2012). The p52:p52 homodimer binds both κB DNAs; but only in the case of the G/C-centric DNA, p52:p52 homodimer can associate with its specific cofactor Bcl3 (p52:p52:Bcl3 complex) and activate transcription by recruiting histone acetyltransferases. When bound to the A/T-centric DNA, the same p52:p52:Bcl3 complex represses gene transcription through the recruitment of histone deacetylases. It is intriguing that the identity of a non-contacted nucleotide should have such a drastic effect on transcriptional selectivity. Leung et al reported that the transcriptional activity of the RelA:RelA homodimer upon binding to A- and T-centric DNAs are different (Leung et al., 2004). Taken together, these reports strongly suggest that NF-κB transcriptional outcomes are coded within specific κB DNA sequences. Even small changes in the promoter specific κB DNAs, which do not alter the overall NF-κB binding affinity, might alter the gene expression profiles. Although structural studies have revealed a stereochemical mechanism of how NF-κB dimers bind κB DNAs, the effect of DNA conformation on complex formation remains underappreciated and it requires solid understanding of both structure and dynamics of κB DNAs to elucidate such a mechanism.

In the present study, we determined the crystal structures of the p52:p52 homodimer in complex with the PSel-κB DNA and two related DNAs where the central three positions were varied. PSel is a known target gene regulated by the p52:p52:Bcl3 complex in cells, and it contains a G/C-centric κB DNA in the promoter region (Pan and McEver, 1995, Wang et al., 2012). All three complexes revealed a widening of the DNA minor groove in the central region. *In vitro* experiments further demonstrated different thermodynamic and kinetic binding features: the binding of p52:p52 with transcriptional active promoters is driven by entropy with faster kinetics. The combination of structural,

MD simulations, and biochemical studies presented here provides new insights into allosteric control by closely related κB DNAs on NF-κB-dependent transcriptional specificity.

Results

The central base pairs in PSel-κB DNA regulate p52:p52:Bcl3 transcriptional activity

Structures of several NF-κB dimers in complex with various κB DNAs have been reported over the past twenty-five years. In all these structures, the DNA sequences contain A/T-centric κB sites (Supplemental Fig. S2E) (Ghosh et al., 1995, Muller et al., 1995, Cramer et al., 1997, Chen et al., 1998b, Huang et al., 2001, Moorthy et al., 2007, Fusco et al., 2009, Chen et al., 1998a). The PSel-κB DNA (5'-GGGGTGACCCC-3') (the central bp is in red color, bps at ±1 positions are underlined), a natural binding site known to be specifically regulated by the p52:p52:Bcl3 complex (Pan and McEver, 1995, Wang et al., 2012), is distinctive from the canonical κB sites not only at the central position but also the two flanking positions. Whereas p50 and other subunits prefers an A:T at –1 and T:A at +1 positions, such as the MHC-κB site (5'-GGGGATTCCCC-3'), PSel-κB contains T:A and A:T at the equivalent positions, respectively. We mutated the central and flanking bps to generate PSel (mutant A/T) and (–1/+1 swap) DNAs. Transcriptional activity of the p52:p52:Bcl3 complex was measured for these three and MHC-κB sites using a luciferase reporter based assay. The natural PSel luciferase reporter could be activated by endogenous NF-κB with co-expression of Bcl3 followed by LPS stimulation (Fig. 1A). To investigate the effects of PSel (mutant A/T) and (–1/+1 swap) on transcriptional activity, luciferase reporter constructs with the variants or MHC-κB site were co-transfected with p52 and Bcl3 expression plasmids. PSel (mutant A/T) showed 2-fold reduced reporter activity, while both PSel (–1/+1 swap) and MHC-κB showed drastically reduced transcriptional activity as compared to the natural PSel-κB (Fig. 1A; Supplemental Fig. S1C). These results suggest that the bp identity at all three positions in the central region are critical in determining transcriptional activity of the p52:p52:Bcl3 complex, which is in line with our previous study that the central bp of κB DNAs plays critical roles in transcriptional regulation (Wang et al., 2012).

Widened minor groove in PSel-κB DNA in complex with NF-κB p52:p52 homodimer

Since only p52 mediates DNA interactions in the p52:p52:Bcl3 complex (Supplemental Fig. S1D) (Bours et al., 1993), we focused our study on (p52:p52)-DNA and speculated that the observed transcriptional differences could be due to different structural features of (p52:p52)-DNA complexes. We solved the crystal structures of p52:p52 homodimer in complex with all three PSel-κB DNAs (Fig. 1C-H; Table 1). The p52 protein works as a bridging factor between target DNAs and Bcl3; therefore, a recombinant p52 protein (aa 1-398) which could form complex with Bcl3 was co-crystallized with the DNAs (Supplemental Fig. S1E-H). This p52 construct contains most of the GRR region which was not included in any previous NF-κB structures (Supplemental Fig. S1B, S2E); however, no electron density was observed for the C-terminal part (aa 330-398) in the structures.

The overall structures of p52:p52 in complex with the natural PSel-κB DNA and two variants are similar to each other (Fig. 1D, H). However, compared to previously known structures of NF-κB-DNA complexes, two striking differences are observed. One is that all three PSel-κB DNAs exhibited a distinct widening of the minor groove at the two base-steps around the central position 0 (–1 to 0 and 0 to +1), with width of ~7.5 Å (Fig. 1E-G, I). In comparison, the A/T-centric κB DNAs studied earlier, κB-33 (5'-GGAAATTTCC-3') (Chen et al., 1998b, Huang et al., 2005) and another one that we now name κB-55 (5'-GGGAATTCCC-3') (Moorthy et al., 2007, Fusco et al., 2009), have significantly compressed minor groove in both their bound and free states as compared to an ideal B-form DNA (Fig. 1I; Supplemental Fig. S2A-B). Compressed minor groove width (MGW) is a common feature of all A/T-centric κB DNAs bound to NF-κB dimers which is remarkably different from the MGW of the PSel-κB DNAs seen in the present structures (Supplemental Fig. S2E).

The widened minor groove is observed with long p52 proteins

The other difference observed for the three p52:p52 structures reported here concerns the organization of the dimer and the complex with DNA. The p52-MHC-κB DNA (which is A/T-centric) complex is the only previously determined crystal structure of NF-κB p52:p52 homodimer (Cramer et al., 1997). Superposition of the p52:p52 homodimer in the MHC-κB and natural PSel-κB complexes aligned by the DDs reveals large rigid body movement of NTDs with rotation of ~20° and translation along rotation axis of ~1.4 Å (Fig. 2A). This results in shifting of the NTD along PSel DNA toward its flanks by ~13 Å for both sides. In addition, the minor groove of the MHC-κB DNA at the

central segment is compressed like all other NF-κB-DNA complexes indicated above (Fig. 1I; Supplemental Fig. S2C).

The PSel-κB DNAs (18 bp) and recombinant p52 protein (aa 1-398, including the GRR) used in the current study are both longer than those in the MHC-κB DNA complex (13bp and aa 35-329). In fact, all currently available structures of NF-κB-κB DNA complexes in the Protein Data Bank (PDB) contain short NF-κB proteins (only NTD and DD) and A/T-centric κB DNAs (Supplemental Fig. S2E) (Ghosh et al., 1995, Muller et al., 1995, Cramer et al., 1997, Chen et al., 1998b, Huang et al., 2001, Moorthy et al., 2007, Fusco et al., 2009, Chen et al., 1998a). To test if the DNA and protein length variations induce structural changes in the complex, we crystallized a 13bp PSel (mutant A/T) DNA bound to a shorter p52 protein (aa 1-327). The conformation of this complex is nearly identical to p52-MHC-κB complex with MGW less than 4 Å at the central position (Fig. 2B, 1I; Supplemental Fig. S2D). This crystal with short p52 is in a different crystal form compared to the three structures with the long p52, and it is also in a different crystal form compared to the MHC-κB DNA complex, suggesting that crystal packing is unlikely to be the main cause of the structural differences, and that both the DNA and protein lengths play significant roles.

Therefore, our structures demonstrate a correlation between the length of the p52 protein and the conformation of the κB DNA and the organization of the p52:p52 dimer in the complex. As discussed above, the short p52 protein (aa 1-327) failed to interact with Bcl3 (Supplemental Fig. S1E-H), partly due to the lack of the GRR. We used the long p52 protein (aa 1-398) for the rest of the studies.

Distinct protein-DNA interactions in the p52:p52-DNA complexes

The widening of the minor groove propagates from the central position to all four base steps on both sides with values around 5-6 Å (Fig. 1I). This widening and the consequent deepening of the major groove have significant impact on protein-DNA interactions. The most significant of which is the loss of cross-strand base contacts by Arg52 (Fig. 3A). The cross-strand contacts between the homologous Arg (Arg54 in p50 and Arg33 in RelA) and DNA is observed in all other A/T-centric NF-κB-DNA structures (Fig. 3B; Supplemental Table S1).

The other notable feature of the PSel-κB DNA complexes is the highly asymmetric DNA contacts by p52:p52 homodimer. Monomer I is closer to its cognate half-site making more direct contacts with the DNA than monomer II (Supplemental Fig. S3A).

Although asymmetric DNA binding by the symmetric homodimer is a common feature in all NF-κB-DNA complexes, it is significantly more pronounced in the present structures. Moreover, the p52:52 homodimer also displays substantial asymmetry. With the DD of the two monomers in superposition, the NTDs rotate from each other by ~6° (Fig. 2C). The interdomain interaction is extensive in monomer I compared to that in monomer II (Fig. 2D).

In the PSel-κB complex, the side chains of Lys221, Arg52, Arg54 and His62 in p52 monomer I make direct base-specific contacts to four consecutive G(s) from +2 to +5 positions (Fig. 3C, Left). In addition, Ser61 also makes direct contact with A at ±6 and ±7 positions; these contacts are not possible for the short p52 (aa 1-327) co-crystallized with 13bp κB DNAs such as MHC and PSel (mutant A/T)-κB (Supplemental Fig. S3A-B). p52 monomer II makes contact with only three G(s) from position –3 to –5 (Fig. 3C, Right). The conformation of loop L3 in the two p52 monomers are different; consequently, only Lys221 in monomer I makes specific contacts with G at position +2 (Supplemental Fig. S3C). Glu58 helps to position Arg52, Arg54 and His62, and makes base-specific interaction to the opposite C at ±3 position.

In addition to base-specific interactions, there are multiple protein contacts to the DNA phosphate backbone, mostly to the central region of the DNA. The side chain of Cys57 hydrogen bonds to the backbone phosphate group of C at ±2; and the side chains of Tyr55 and Lys143 hydrogen bond to the backbone phosphate group of A at ±1. Only in monomer II does the side chains of Lys143 make an additional hydrogen bond (H-bond) to the backbone phosphate group of C at position 0 (Fig. 3D). Interestingly, all other NF-κB-DNA complexes, including the short p52:p52 homodimer bound to both 13bp MHC-κB and PSel (mutant A/T)-κB DNAs, exhibit more backbone contacts by Gln284 and Gln254 (Supplemental Fig. S3B; Supplemental Table S1). The presence of an additional positively charged residue in loop L2 in the other NF-κB subunits (p52: T^{142}KKN; p50: TKKK; and RelA: KKRD) enhances backbone binding at the minor groove side including cross-strand interactions (Fig. 3E). In addition, there is a unique basic segment in p52, a peptide rich in basic residues (K^{179}ELKK), located near the end of helix α2 (Fig. 3E). These basic residues possibly mediate long-range electrostatic interactions with the negatively charged DNA backbone which might pull the DNA strands away from each other towards the p52 protein (Fig. 3F). In summary, amino acid composition in loop L2 and helix α2 might play an important role in determining DNA

binding by the NF-κB dimers.

MD simulations reveal free DNAs exist in distinct preferred conformations

In order to investigate whether MGW of the PSel-κB DNA variants observed in the current complexes is induced by the protein or it is intrinsic to DNA sequences, we carried out microsecond-long MD simulations for the four κB DNAs in free form. The simulations started from the DNA conformation in the crystal structures of the complexes, with the three PSel-κB DNA variants having a widened minor groove and the MHC-κB DNA having a narrow minor groove. At the end of the simulation, PSel (natural G/C-centric) and (mutant A/T-centric) maintained the widened minor groove, while PSel (−1/+1 swap) displays a narrow minor groove at the central 0 position similar to MHC-κB DNA in the simulations (Fig. 4A). The swap of T and A at ±1 positions reverses the geometric conformation of bps at both positions (Fig. 4C). Specifically, these swaps cause an opposite orientation of each nucleotide, forcing the bps to adopt an opposite shear and buckle direction compared to those on the non-swapped DNAs. The thymine at both positions slides and tilts towards the minor groove simultaneously, narrowing the central minor grooves (Supplemental Fig. S4A).

The simulations also reveal a narrowed minor groove of the A/T-centric DNA at +1 position compared to the corresponding G/C-centric DNA with the same flanking bps, i.e. PSel (mutant A/T-centric) compared to PSel (natural G/C-centric), and MHC compared to PSel (-1/+1-swap) (Fig. 4B). The A:T bp at 0 position shows large shear, buckle and opening, forcing a register towards the minor groove in the curvature of free A/T-centric DNAs (Supplemental Fig. S4A). This conformation orients the thymine towards the minor groove and might have caused the decrease in MGW at +1 position. Collectively, having A:T at N position or T:A at N+2 position is likely to intrinsically reduce the MGW at N+1 position. Our finding is in line with the observations of compressed minor groove of free κB-33 DNA or the bending into minor groove from continuous A:T in A-tract DNAs (Barbič et al., 2003).

Comparison of MD simulations and crystal structures suggests that upon binding to p52 the −1/+1 swap DNA experiences more disruptive conformational change than the natural G/C-centric PSel-κB (Fig. 4A; Supplemental Fig. S4B). The binding at the central part of both DNAs is symmetrically facilitated through the H-bonds between two residues (Lys143 and Tyr55) from each monomer of p52 and the phosphate of nucleotides at −1 and +1 and T-shaped π-stacking interactions between DNA bases and Tyr55. These two

residues in the two p52 monomers are positioned further apart in the PSel-κB DNA complex compared to the MHC-κB DNA complex. Unlike the natural G/C-centric DNA, the bindings on both strands of −1/+1 swap DNA draw the bound thymine in the opposite direction of the minor groove, breaking the intra-bp H-bonds and severely distorts the central bps (Supplemental Fig. S4B). It appears that p52:p52 homodimer adopts a specific conformation with a nearly fixed inter-monomer distance upon the binding to κB DNAs, such that it tears the central part of −1/+1 swap DNA into a favored binding conformation. Overall, the comparative analysis of MD simulations and crystal structures suggests that the p52:p52 homodimer induces the least amount of conformational changes on κB DNA with an intrinsically widened minor groove.

The p52 homodimer recognizes κB DNAs with different thermodynamic features

Structural analysis described above did not provide a strong correlation between the conformational states of (p52:p52)-DNA complexes and the transcriptional output. We next tested whether p52:p52 homodimer binds to the natural G/C-centric, mutant A/T-centric, and −1/+1 swap PSel-κB, as well as MHC-κB DNAs with different mechanisms and/or affinities. In all cases, long p52 protein (aa 1-398) as well as long DNA were used. Isothermal titration calorimetry (ITC) reveals that p52:p52 binds all three PSel-κB DNA variants with similar binding affinities (K_d) of approximately 70 nM whereas it binds MHC-κB DNA more than 2-fold tighter (Fig. 5A-D). However, binding of p52 to the natural G/C-centric PSel-κB DNA is associated with a large increase in entropy (ΔS), while the binding to the MHC-κB DNA showed a large decrease in entropy. On the other hand, the binding to the MHC and mutant A/T-centric PSel DNAs showed a much larger decrease in enthalpy (ΔH). These results suggest that the binding of p52:p52 homodimer to the G/C-centric κB DNA is favored by entropy, whereas the binding to the A/T-centric DNA is driven by enthalpy.

To test if this mechanism is general to other κB DNAs, we also determined the thermodynamic parameters for p52 binding to Skp2-κB DNA. Skp2-κB DNA is present in the promoter of S-phase kinase-associated protein 2 (Skp2) and it is also regulated by the p52:p52 homodimer and Bcl3 (Supplemental Fig. S5A) (Barre and Perkins, 2007, Wang et al., 2012). Skp2-κB DNA is another natural G/C-centric (5'-GGGGAGTTCC-3') κB DNA but with the presence of A:T and T:A bp at +1 and −1 positions, the same as the −1/+1 swap PSel DNA in the central region. Skp2 also has a very different 4bp half-site, TTCC, at the +1 to +4 positions. The K_d as well as relative contributions of entropy and

enthalpy to the binding to Skp2 and −1/+1 swap PSel DNAs are similar (Fig. 5C; Supplemental Fig. S5B). These results suggest that DNA sequence and conformational differences lead p52 to bind DNAs through different thermodynamic binding processes. However, thermodynamic binding mechanism does not fully capture the differential transcriptional output mediated by these κB DNAs.

The p52 homodimer binds κB DNAs with different kinetic features

We next examined the binding kinetics of p52 and κB DNAs as there is mounting evidence that, separate from binding affinity, kinetic rate constants (k_{on} and k_{off}) are crucial to the physiological effects of protein-ligand interactions in a variety of cellular processes (Nakajima et al., 2001, Gross and Lodish, 2006, Gonzalez et al., 2005, Markgren et al., 2002). We utilized biolayer interferometry (BLI) to study the association and dissociation rate of p52:p52 binding to various κB DNAs. Biotinylated DNAs were immobilized on the streptavidin (SA) sensors and tested with purified p52 protein. The binding kinetics differ significantly among the DNAs. The binding of more transcriptionally active natural G/C-centric PSel showed a higher association (k_{on}) and dissociation rate (k_{off}) than the other two variants and MHC-κB DNAs (Fig. 6A-E). Consistently, in the case of Skp2-κB DNA, the more transcriptionally active natural G/C-centric Skp2 showed a faster kinetics than its mutant A/T-centric, especially the k_{off} (Supplemental Fig. S6A-C).

We further determined the k_{on} and k_{off} of the transcriptionally competent p52:p52:Bcl3 complex binding to PSel-κB DNA variants by BLI. In agreement with our previous study, only the recombinant phospho-mimetic Bcl3 from E. coli forms ternary complex with p52:p52 homodimer and κB DNA (Wang et al., 2017). Both recombinant WT and phospho-mimetic Bcl3 protein (S33/114/446E mutant) interact with p52 with similar kinetics (Supplemental Fig. S1F, S7A-C); however, the p52:p52:WT-Bcl3 complex does not bind DNAs (Supplemental Fig. S7D-E). The binding of p52:p52:phospho-Bcl3 with the natural G/C-centric PSel DNA exhibited both higher k_{on} and k_{off} (Fig. 6F-J). Similarly, the binding with the natural G/C-centric Skp2 DNA also showed a higher k_{off} comparing to its A/T-centric mutant (Supplemental Fig. S6D-F).

Overall, the binding kinetics of p52:p52 homodimer alone vs. p52:p52:Bcl3 complex follows the same trend. Moreover, a comparison of binding affinity, association and dissociation rates with respect to the more transcriptionally active PSel and Skp2-κB sites shows a correlation between transcriptional output and the dissociation rate. The

slower the k_{off}, the lower the reporter activities for both (p52:p52)-DNA and (p52:p52:Bcl3)-DNA complexes (Fig. 6K; Supplemental Fig. S6G). Therefore, transcriptional activity may have a closer link to the binding kinetics rather than the thermodynamic stability of the complex.

Discussion

The p52 homodimer recognizes κB DNA using a mode distinct from other NF-κB dimers

Double-stranded DNA helices are not static entities that simply present themselves to proteins and assemble into multiprotein complexes at specific sequences. The DNA duplex is intrinsically dynamic on many levels and time scales in cells. The movement of DNA through its different conformational states is continuous and is influenced by, but not completely dependent upon, its nucleotide sequence. Structures presented in this study show that the conformations of all three PSel-κB DNA variants bound to the long p52:p52 homodimer are similar but are distinct from all previously known complexes between κB DNAs and six other NF-κB dimers (p50:p50, p50:RelA, p50:RelB, RelA:RelA, c-Rel:c-Rel and p52:RelB). It was noted earlier a compressed minor groove in the central region of the DNA is a key feature of NF-κB-DNA complexes. The minor groove at the central three positions is significantly widened in all three complexes presented here. However, MD simulations show free DNAs exist in distinct preferred conformations, which appears to be adjusted by p52 into a unique shape for recognition. And notably, the more transcriptionally active natural PSel-κB DNA appears to maintain similar conformational and dynamic states in free and bound forms.

The current structures also demonstrate a correlation between the p52 protein length and the conformation of the κB DNA. The GRR region of the p52 protein, which was not included in any previous NF-κB structural studies, seems to play an important role. However, no electron density was observed for the GRR region in the current structures. Future studies are needed to fully understand the role of the GRR region in (p52:p52)-DNA complex conformation and the interaction with cofactor Bcl3.

Binding affinity does not fully capture the transcriptional activity

To determine if binding affinity is related to transcriptional activity, we measured the affinity of all complexes under equilibrium condition. Surprisingly, but consistent with our previous report (Mulero et al., 2018), we found no correlation between affinity and

transcriptional activity. The p52:p52 homodimer binds to MHC-κB with the highest affinity but it is not a transcriptional activation competent complex. Interestingly, our analysis reveals that p52:p52 homodimer uses different paths to bind κB DNAs ranging from purely entropic for the natural PSel, to exclusively enthalpic for MHC, and to mixed entropic-enthalpic for mutant A/T-centric and −1/+1 swap PSel DNAs. The entropy-driven processes are linked to faster binding kinetics: p52:p52 homodimer binds to natural G/C-centric PSel DNA with both faster association and dissociation rates. The most populated conformation of the free G/C-centric PSel DNA as revealed by MD simulation is similar to the one observed in the crystal structure of the complex suggesting this DNA's conformation does not undergo significant changes upon protein binding. Thus, in the complex between p52:p52 and natural G/C-centric DNA, both the DNA and protein most likely preserve their native states. This could account for the positive entropy and faster k_{on}. However, possibly protein-DNA contacts in such a complex are sub-optimal resulting in their faster dissociation. In contrast, p52:p52 complexes with the mutant A/T-centric or −1/+1 swapped DNAs likely involve rigidification of protein-DNA contacts, requiring some structural reorganizations in both molecules, results in more enthalpically stable complexes and slower association and dissociation rates. Combination of MD simulations and structural studies supports this model as PSel (mutant A/T) and (−1/+1 swap) DNAs undergo conformational changes from free to bound states. Our observations are consistent with other studies which showed rapid association and dissociation is favored by entropy, whereas slow association and dissociation is guided by enthalpy (Baerga-Ortiz et al., 2004).

Ideas and Speculation: Transcriptional regulation via kinetic discrimination

Understanding transcriptional regulation has attracted many researchers since the discovery of the *lac* operon. One of the most intriguing questions scientists are working to resolve is the mechanism of transcriptional regulation by the specific DNA response elements. Affinity regulation by different target DNA sequences for a TF has long been thought to be the dominant mode of regulation imposed by such DNA sequences. Indeed, in many cases of eukaryotic transcription differential affinity has been shown to be critical (Sekiya et al., 2009). TFs are also known to bind free DNA or nucleosome with distinct kinetics (Donovan et al., 2019). But none of these studies has established a direct correlation between binding kinetics and transcriptional regulation in eukaryotes. Many biological systems have been studied in detail with the roles of binding kinetics in

regulation evaluated. For instance, receptor ligand interactions, T cell activation and potency of bacterial toxins are guided by the half-life of key complexes (Corzo, 2006, Gonzalez et al., 2005, Gross and Lodish, 2006, Nakajima et al., 2001).

Of all six κB DNAs tested, the natural G/C-centric PSel and Skp2 DNAs showed greater transcriptional activation. We found that a slower dissociation rate or longer residence time is linked to reduced transcriptional activation. Although the relationship between the dissociation rates and transcription activities is shown for only six tested binding sites, this relationship is preserved for (p52:p52)-DNA complexes and to a lesser extent for (p52:p52:Bcl3)-DNA complexes.

The rate constants obtained in our *in vitro* assays probably are not the same *in vivo*, where many other factors will have an impact on binding kinetics. However, the relative rates clearly suggest that the persistent presence of p52 on DNA gives rise to less transcription. Work presented here hints at a link between the DNA binding kinetics of a TF and its interaction with coactivators and corepressors. We previously showed that the p52:p52:Bcl3 complex preferentially recruits HDAC3 when it remains bound to an A/T-centric κB site (Wang et al., 2012), it is possible that the slower dissociation rate or longer residence time of p52:p52:Bcl3 on the A/T-centric κB site described in this study matches the slower on rate of the corepressor to p52:p52:Bcl3 bound to A/T DNA. That is, the A/T-centric κB DNA:p52:p52:Bcl3 complex remains stable for long enough to give the HDAC3 corepressor complex enough time to stably interact with it. In addition, the binding of other TFs to the promoters/enhancers of target genes inevitably impacts on the coactivator/corepressor regulation by the (p52:p52)-DNA complexes. Future experiments aimed at coactivator and corepressor interaction rates within the context of chromatinized DNA are needed to verify the validity of the kinetic model for DNA element sequence-specific gene regulation.

In summary, our studies have revealed a novel conformation for κB DNA in complex with NF-κB and a new organization of an NF-κB dimer. More importantly, our work provides a new insight into the mechanism of differential thermodynamics and kinetics of NF-κB-DNA binding. DNA response elements with only one or two bp variations could provoke drastically different kinetic and thermodynamic effects. Future experiments will help us fully understand how such binding processes result in transcription activation or repression.

Materials and Methods

Protein expression and purification

Recombinant non-tagged human p52 (1-398) and (1-327) was expressed and purified from *Escherichia coli* Rosetta (DE3) cells. Rosetta (DE3) cells transformed with pET-11a-p52 (1-398) or (1-327) were cultured in 2 L of LB medium containing 50 mg/mL ampicillin and 34 mg/mL chloramphenicol at 37 ^{o}C. Expression was induced with 0.2mM Isopropyl β-D-1-thiogalactopyranoside (IPTG) at OD_{600} 0.5-0.6 for 3 hours. Cells were harvested by centrifugation, suspended in 40 mM Tris-HCl (pH 7.5), 100 mM NaCl, 10 mM β-ME, 1 mM PMSF, and lysed by sonication. Cell debris was removed by centrifugation (20,000 g for 30 min). Clarified supernatant was loaded onto Q-Sepharose FF column (GE Healthcare). Flow-through fraction was applied to SP HP column (GE Healthcare). The column was washed with 40 mM Tris-HCl (pH 7.5), 200 mM NaCl; 10 mM β-ME, and the protein was eluted by the same buffer containing 400 mM NaCl. p52 was concentrated and loaded onto the gel filtration column (HiLoad 16/600 Superdex 200 pg, GE Healthcare) pre-equilibrated with 10 mM Tris-HCl (pH 7.5), 100 mM NaCl; 5 mM β-ME. Peak fractions were concentrated to ~10 mg/mL, flash frozen in liquid nitrogen and stored at -80°C. His-Bcl3 (1-446) WT and phospho-mimetic mutant was expressed in *Escherichia coli* Rosetta (DE3) cells by induction with 0.2 mM IPTG at OD_{600} 0.4 for 8 hours at 24°C. Cell pellets of 2 L-culture of Bcl3 alone or together with 1 L-culture of p52 (for p52:Bcl3 complex) were resuspended together in buffer containing 20 mM Tris-HCl (pH 8.0), 300 mM NaCl, 25 mM imidazole, 10% glycerol, 10 mM β-ME, 0.1 mM PMSF and 50μL protease inhibitor cocktail (Sigma) and then purified by Ni Sepharose (HisTrap HP, GE) followed by anion exchange column (Q Sepharose fast flow, GE). The protein complex further went through HiTrap Desalting Column (GE) to exchange buffer before BLI assays.

Crystallization, data collection, and structure determination

Annealed DNA duplex was mixed in 20% molar excess with the pure protein.

The crystals of the p52(aa 1-398):PSel(G/C-centric) 18bp complex were obtained by the sitting-drop vapor diffusion method at 20 °C with a reservoir solution containing 0.1 M sodium malonate (pH 4.0), 0.2 M CsCl and 5% (w/v) PEG 3350.

The crystals of the p52(aa 1-398):PSel(A/T-centric) 18bp complex, and the p52(aa 1-398):PSel(−1/+1 swap) 18bp complex were obtained by the sitting-drop vapor diffusion method at 20 °C with a reservoir solution containing 0.1 M sodium malonate (pH 4.0), 50 mM CsCl and 2.5% (w/v) PEG 3350.

The crystals of the p52(aa 1-327):PseI(A/T-centric) 13bp complex were obtained by the sitting-drop vapor diffusion method at 20 °C with a reservoir solution containing 50 mM MES (pH 6.0), 10 mM $MgCl_2$ and 10% (w/v) PEG 3350.

Before data collection, all crystals were briefly soaked in their original crystallization solution with 20% (v/v) ethylene glycol. All crystals were flash frozen in liquid nitrogen for diffraction screening and data collection at 100 K. X-ray diffraction data were collected at beamline BL19U1 at Shanghai Synchrotron Radiation Facility. The initial solution was obtained by molecular replacement using Phaser (McCoy et al., 2007) with p52-MHC DNA complex (Cramer et al., 1997) as the search model. The structure was further refined through an iterative combination of refinement with Refmac5 (Murshudov et al., 2011) and manual building in the Coot program (Emsley and Cowtan, 2004, Emsley et al., 2010). The crystallographic information is summarized in Table 1.

MD simulation

All MD simulations were carried out in GROMACS 2020.6 (Lindahl et al., 2020) with Amber14sb force field (Maier et al., 2015) and OL15 parameters for DNA (Zgarbová et al., 2015). Crystal structures of κB/κB-like DNAs were extracted from the resolved p52-bound structures, where the MHC DNA was retrieved from RCSB PDB database (PDB 1A3Q) (Cramer et al., 1997). In each system, κB DNA was placed in the center of a dodecahedron box with a 12-Å margin, solvated with TIP3P water (Jorgensen et al., 1983), and ionized with 0.1 M NaCl. Energy minimization was performed until the maximum force of system was below 1,000 $kJ \cdot mol^{-1} \cdot nm^{-1}$. The minimized system was then equilibrated in a NVT ensemble for two 1-ns stages, positionally restraining the DNA heavy atoms with a force constant of 20,000 $kJ \cdot mol^{-1} \cdot nm^{-2}$ and 10,000 $kJ \cdot mol^{-1} \cdot nm^{-2}$, respectively. Subsequently, the system was subjected to a 6-ns position-restrained NPT equilibration, with the force constant gradually reduced from 10,000 $kJ \cdot mol^{-1} \cdot nm^{-2}$ to 400 $kJ \cdot mol^{-1} \cdot nm^{-2}$. Finally, five replicas of 2-μs unrestrained production simulations were run for each well-equilibrated DNA system, resulting in an aggregated 10-μs trajectory for each system. In all simulations, van der Waals forces were smoothly switched to zero from 9 Å to 10 Å. Electrostatics were calculated using the particle mesh Ewald (PME) method (Darden et al., 1993) with a cutoff of 10 Å. A velocity-rescaling thermostat (Bussi et al., 2007) was employed for the temperature coupling at 300 K, whereas pressure coupling at 1 bar was implemented by a Berendsen barostat (Berendsen et al., 1984).

All bonds involving H atoms were constrained using the LINCS algorithm (Hess et al., 1997).

Occupancy of DNA was calculated over the aggregated integrated 10-μs trajectories using the VolMap tool in VMD (Humphrey et al., 1996). The clustering analyses were conducted within GROMACS packages using GROMOS method. Representative structures of DNA and bp at position −1, 0, +1 were obtained from the centroid structures of top clusters and rendered with PyMOL (Schrodinger, 2015). The hydrogen bonds were calculated using PyMOL with default standard (heavy atom distance cutoff of 3.6 Å and angle cutoff of 63°). The bp and groove parameters were measured via Curves+ (Lavery et al., 2009, Blanchet et al., 2011), with the uncertainty represented by the standard error of the mean (SEM) computed from the five replica simulations of a given system.

Isothermal titration calorimetry (ITC) assays

ITC measurements were carried out on a MicroCal iTC200 (Malvern Inc.) at 25°C. The ITC protein sample p52 (1-398) went through desalting column (HiTrap desalting, GE Healthcare) to freshly made ITC buffer containing 20 mM Tris-HCl (pH 8.0), 100 mM NaCl, 1mM dithiothreitol (DTT). 35 μM p52 (1-398) protein (in cell) was titrated with 300 μM DNAs (in syringe). A time interval of 150 seconds between injections was used to ensure that the titration peak returned to the baseline. The titration data were analyzed using the program Origin7.0 and fitted by the One Set of Site model.

Biolayer interferometry (BLI) assays

The kinetic assays were performed on Octet K2 (ForteBio) instrument at 20°C with shaking at 1000 RPM. The streptavidin (SA) biosensors were used for protein-DNA interactions and were hydrated in BLI buffer containing 20 mM Tris-HCl (pH 8.0), 100 mM NaCl, 1 mM DTT and 0.02% (v/v) Tween-20. All DNAs used were 20-mer in length and biotin-triethyleneglycol (TEG) labelled. The DNAs were loaded at 50 nM for 300 sec prior to baseline equilibration for 60 sec in the BLI buffer. Association of p52:p52 (aa 1-398) or p52:p52:Bcl3 complex in BLI buffer at various concentrations was carried out for 400 sec prior to dissociation for 600 sec. The Ni-NTA biosensor were used for protein-protein interactions and were hydrated in BLI buffer containing 20 mM Tris-HCl (pH 8.0), 200 mM NaCl, 5% glycerol, 1 mM DTT and 0.02% (v/v) Tween-20. His-tagged-Bcl3 was loaded at 500 μg/mL for 90 sec prior to baseline equilibration for 180 sec in the BLI buffer. Association of p52 in BLI buffer at various concentrations was carried out for 240

sec prior to dissociation for 360 sec. All data were baseline subtracted and analyzed in ForteBio data analysis software using a global fitting to a 1:1 binding model. The experiments were done in duplicate.

Luciferase Reporter Assays

HeLa cells were transiently transfected with Flag-p52(1-415) together with Flag-Bcl3(1-446) expression vectors or empty Flag-vector, and the luciferase reporter DNA with specific κB DNA promoter (Wang et al., 2012). The total amount of plasmid DNA was kept constant for all assays. Transient transfections were carried out using Lipofectamine 2000 (Invitrogen). Cells were collected 48 hours after transfection. Luciferase activity assays were performed using Dual-Luciferase Reporter Assay System (Promega) following the manufacturer's protocol. Data are represented as mean standard deviations (SD) of three independent experiments in triplicates.

Data Availability

The atomic coordinates have been deposited in the Protein Data Bank, www.wwpdb.org (PDB ID codes 7CLI, 7VUQ, 7VUP and 7W7L).

Acknowledgments

We thank the Proteomics, Metabolomics and Drug Development (PMDD) core at Faculty of Health Sciences for providing the ITC machine for the thermodynamic assays. We thank the staffs from BL19U1 beamline of National Facility for Protein Science in Shanghai (NFPS) at Shanghai Synchrotron Radiation Facility, for assistance during data collection. We thank Prof. Liang Tong at Columbia University for critical discussion of the manuscript. This work was supported by the Science and Technology Development Fund, Macao S.A.R. (FDCT) [project 0104/2019/A2 to V.Y.-F.W.]; the Multi-Year Research Grant from University of Macau [MYRG2018-00093-FHS to V.Y.-F.W.]. T.L. and Y.W. were supported by direct grants from the Chinese University of Hong Kong. G.G. were supported by the National Institutes of Health (NIH) [GM085490 and CA142642 to G.G.].

Author Contributions: V.Y.-F.W. designed the experiments and supervised the project. V.M. performed the complex crystallization, structure determination and refinement. W.P. carried out all the biochemistry, thermodynamic and binding kinetic studies. T.L. performed MD simulation. V.M., W.P., T.L., Y.W., G.G. and V.Y.-F.W. analyzed the data. V.Y.-F.W., G.G., W.Y. and T.L. wrote the paper.

Declaration of interests

The authors declare no competing interests.

Figures Legends

Figure 1. Crystal structures of p52:p52 homodimer in complex with PSel-κB DNA variants reveal distinct signatures. (A) The natural G/C-centric PSel luciferase reporter was activated by endogenous NF-κB with LPS stimulation and Bcl3 co-expression. The data were analyzed from three independent experiments performed in triplicate. RLU, relative luciferase unit. *p<0.05; **p<0.01 (t test). Error bars represent standard deviation (SD). (B) Luciferase reporter activity driven by co-expression of p52 and Bcl3 was reduced when the natural G/C-centric PSel site was mutated to A/T-centric or −1/+1 swap sites; and the MHC luciferase reporter was not activated by p52:p52:Bcl3 complex. The data were analyzed from three independent experiments performed in triplicate. *p<0.05; **p<0.01; ***p<0.001; n.s., not significant (t test). Error bars represent SD. (C) Overall structure of p52:p52 in complex with the natural G/C-centric PSel-κB DNA. (Left) Ribbon diagram showing the entire complex viewed down the DNA helical axis. The two p52 monomers are shown in orange (monomer I) and green (monomer II), respectively; and the DNA duplex is shown in blue; (Right) View of the complex after rotating 90° along the vertical axis. (D) Overlay p52:p52 homodimers in three PSel-κB DNA variants by their dimerization domain (DD). Monomer I is shown in tv_orange, bright orange and light orange; monomer II is shown in forest, tv_green and lime in the natural G/C-centric, mutant A/T-centric and −1/+1 swap complexes. All three structures are presented as backbone traces. (E-G) Structure of the 18bp PSel-κB DNAs with (E) natural G/C-centric (blue), (F) mutant A/T-centric (light pink) and (G) −1/+1 swap (ruby). The DNA bps as observed in the co-crystal structures are shown in filled sticks. The view is onto the central minor groove. The nucleotide sequences used in co-crystallization are shown at the bottom, with κB DNA underlined and numbering scheme indicated above; the central position 0 is highlighted in red, and the swap of −1 and +1 positions is highlighted in green. (H) Overlay of natural G/C-centric, mutant A/T-centric, and −1/+1 swap PSel-κB DNAs in (E-G). (I) Table showing minor groove widths and major groove depths (Å); the ideal B-form DNA was built using Coot program (Emsley and Cowtan, 2004, Emsley et al., 2010) based on the sequence of PSel-κB DNA. The minor groove widths at the central region from position −1 to +1 are shown in red, and the corresponding major groove depths are shown in green. Geometrical parameters and the helical axes were calculated with Curves+ (Blanchet et al., 2011, Lavery et al., 2009).

Figure 2. p52:p52 dimer conformations. (A) (Left) Overlay of p52:p52 (aa 1-398) in complex with the 18bp natural G/C-centric PSel-κB DNA (PDB 7CLI, this study)(in

orange and green for monomer I and II, respectively) and p52:p52 (aa 35-329) in complex with the MHC-κB DNA (PDB 1A3Q)(in gray). Diagram explains rigid-body movement of the NTD. (Right) View of the complex after rotating 90° along the horizontal axis. Both protein structures are presented as backbone traces. (B) Overlay of the short p52:p52 (aa 1-327) in complex with the 13bp PSel(mutant A/T)-κB DNA (PDB 7W7L, this study)(in yelloworange and purpleblue for monomer I and II, respectively) and p52:p52 (aa 35-329) in complex with the MHC-κB DNA (PDB 1A3Q)(in gray). (C) Conformational differences between two p52 monomers in complex with the 18bp natural G/C-centric PSel-κB DNA (PDB 7CLI, this study) are shown by superposing their DDs. The two monomers are presented as backbone traces. (D) Hydrogen bonding network at the interdomain interface between DD and NTD in each p52 monomer. In monomer I, the two domains form contacts with each other through a wide network of H-bonds between the side chains of Arg49 from the NTD and Gly224, Ser226, Arg311 and Asp316 from the DD; whereases in monomer II, there are only contacts between Arg49 and Ala225, as well as Ser226 and Arg311.

Figure 3. Protein-DNA contacts. (A) Arg52 of p52 in the PSel-κB complex (PDB 7CLI, this study) only makes base-specific contacts with G at +3 position. (B) The corresponding Arg54 of p50 in the p50:RelA-IFNb-κB complex (PDB 1LE5) makes base-specific contacts with A at –2 and G at –3 positions as well as additional cross-strand contacts with T at –2 position. (C) DNA based-specific contacts made by Arg52, Arg54, His62 and Lys221 of p52 (Left) monomer I and (Right) monomer II in complex with the natural PSel-κB DNA. H-bonds are indicated as red dotted lines with distances labelled. Noted that Lys221 in monomer II is in a different conformation and has no specific contacts with DNA. (D) DNA backbone contacts made by Lys143 of p52 (Left) monomer I and (Right) monomer II. (E) Sequence alignment showing the unique basic segment in p52 among all NF-κB family members. Both human and mouse sequences of the p52 subunit are shown. Only human sequences are shown for the rest of the family members. Secondary structures and connecting loops are drawn above the sequences. (F) (Left) The unique basic segment in p52 NTD helix a2 interacts with PSel-κB DNA in the present structure (PDB 7CLI, this study); (Right) these interactions are absent in p50 subunit in the p50:RelA-IFNb-κB complex (PDB 1LE5).

Figure 4. MD simulations for free κB DNAs. (A-B) Statistical MGW over the aggregated 10-μs simulations of each system at (A) the central 0 position (averaged over the five

682 levels from –1 to +1 positions) and (B) the +1 position (averaged over the five levels from
683 0 to +2 positions). (Upper) DNA isosurface at 0.2 isovalue (20% occupancy); (Lower)
684 Probability distribution of MGW. Dashed lines show the MGW in the (p52:p52)-bound
685 crystal structures. (C) Representative structures of natural G/C-centric, mutant A/T-
686 centric, –1/+1 swap PSel-κB DNAs and MHC-κB DNA revealed from MD simulations.
687 (Left) Superimposed structures showing the narrowed central minor groove on –1/+1
688 swap DNAs; (Right) Representative conformations of bps at –1, 0 and +1 positions
689 revealed from MD simulations. MGW was calculated with Curves+ (Blanchet et al., 2011,
690 Lavery et al., 2009).

691 **Figure 5.** p52 binds κB DNAs with different thermodynamic features. (A-D) Calorimetric
692 titration data showing the binding of recombinant p52:p52 (aa 1-398) homodimer with (A)
693 natural G/C-centric, (B) mutant A/T-centric, (C) –1/+1 swap PSel-κB and (D) MHC-κB
694 DNAs. The top panel of the ITC figures represent the binding isotherms; the bottom
695 panel shows the integrated heat of the reaction and the line represents the best fit to the
696 data according to a single-site binding model. The determined K_d, changes of enthalpy
697 and entropy are shown on the bottom panel.

698 **Figure 6.** p52 binds the natural transcriptionally active G/C-centric PSel-κB DNA with
699 faster kinetics. (A-D) Biolayer interferometry (BLI) binding analysis of p52:p52 (aa 1-398)
700 homodimer to immobilized biotin labeled (A) natural G/C-centric, (B) mutant A/T-centric,
701 (C) –1/+1 swap PSel-κB and (D) MHC-κB DNAs. The differences in k_{on} and k_{off} can be
702 seen in the shapes of the association and dissociation curves. Each experiment was
703 done in duplicate and one representative set of curves is shown. (E) Table showing the
704 kinetic analysis in (A-D). (F-I) BLI binding analysis of p52:p52:Bcl3 complex to
705 immobilized biotin labeled (F) natural G/C-centric, (G) mutant A/T-centric, (H) –1/+1
706 swap PSel-κB and (I) MHC-κB DNAs. Each experiment was done in duplicate and one
707 representative set of curves is shown. (J) Table showing the kinetic analysis in (F-I). (K)
708 Table summarizing the fold change of K_d, k_{on} and k_{off} with respect to the more
709 transcriptionally active G/C-centric PSel-κB DNA. The average values of the duplicated
710 kinetics data in (A-J) and the relative reporter activities in RLU from Fig. 1A-B were used
711 for ratio calculations. The numbers for the greater reporter active G/C-centric PSel are
712 shown in blue.

713 **Table 1. Summary of crystallographic information.**

References

ANNUNZIATA, C. M., DAVIS, R. E., DEMCHENKO, Y., BELLAMY, W., GABREA, A., ZHAN, F., LENZ, G., HANAMURA, I., WRIGHT, G., XIAO, W., DAVE, S., HURT, E. M., TAN, B., ZHAO, H., STEPHENS, O., SANTRA, M., WILLIAMS, D. R., DANG, L., BARLOGIE, B., SHAUGHNESSY, J. D., JR., KUEHL, W. M. & STAUDT, L. M. 2007. Frequent engagement of the classical and alternative NF-kappaB pathways by diverse genetic abnormalities in multiple myeloma. *Cancer Cell,* 12**,** 115-30.

BAERGA-ORTIZ, A., BERGQVIST, S., MANDELL, J. G. & KOMIVES, E. A. 2004. Two different proteins that compete for binding to thrombin have opposite kinetic and thermodynamic profiles. *Protein Sci,* 13**,** 166-76.

BARBIČ, A., ZIMMER, D. P. & CROTHERS, D. M. 2003. Structural origins of adenine-tract bending. *Proceedings of the National Academy of Sciences,* 100**,** 2369-2373.

BARRE, B. & PERKINS, N. D. 2007. A cell cycle regulatory network controlling NF-kappaB subunit activity and function. *EMBO J,* 26**,** 4841-55.

BERENDSEN, H. J. C., POSTMA, J. P. M., GUNSTEREN, W. F. V., DINOLA, A. & HAAK, J. R. 1984. Molecular dynamics with coupling to an external bath. *The Journal of Chemical Physics,* 81**,** 3684-3690.

BERKOWITZ, B., HUANG, D. B., CHEN-PARK, F. E., SIGLER, P. B. & GHOSH, G. 2002. The x-ray crystal structure of the NF-kappa B p50.p65 heterodimer bound to the interferon beta -kappa B site. *J Biol Chem,* 277**,** 24694-700.

BLANCHET, C., PASI, M., ZAKRZEWSKA, K. & LAVERY, R. 2011. CURVES+ web server for analyzing and visualizing the helical, backbone and groove parameters of nucleic acid structures. *Nucleic Acids Res,* 39**,** W68-73.

BOURS, V., FRANZOSO, G., AZARENKO, V., PARK, S., KANNO, T., BROWN, K. & SIEBENLIST, U. 1993. The oncoprotein Bcl-3 directly transactivates through kappa B motifs via association with DNA-binding p50B homodimers. *Cell,* 72**,** 729-39.

BUSSI, G., DONADIO, D. & PARRINELLO, M. 2007. Canonical sampling through velocity rescaling. *J Chem Phys,* 126**,** 014101.

CHEN, F. E. & GHOSH, G. 1999. Regulation of DNA binding by Rel/NF-kappaB transcription factors: structural views. *Oncogene,* 18**,** 6845-52.

CHEN, F. E., HUANG, D. B., CHEN, Y. Q. & GHOSH, G. 1998a. Crystal structure of p50/p65 heterodimer of transcription factor NF-kappaB bound to DNA. *Nature,* 391**,** 410-3.

CHEN, Y. Q., GHOSH, S. & GHOSH, G. 1998b. A novel DNA recognition mode by the NF-kappa B p65 homodimer. *Nat Struct Biol,* 5**,** 67-73.

CHEN, Y. Q., SENGCHANTHALANGSY, L. L., HACKETT, A. & GHOSH, G. 2000. NF-kappaB p65 (RelA) homodimer uses distinct mechanisms to recognize DNA targets. *Structure Fold Des,* 8**,** 419-28.

CHEN-PARK, F. E., HUANG, D. B., NORO, B., THANOS, D. & GHOSH, G. 2002. The kappa B DNA sequence from the HIV long terminal repeat functions as an allosteric regulator of HIV transcription. *J Biol Chem,* 277**,** 24701-8.

CHENG, C. S., FELDMAN, K. E., LEE, J., VERMA, S., HUANG, D. B., HUYNH, K., CHANG, M., PONOMARENKO, J. V., SUN, S. C., BENEDICT, C. A., GHOSH, G. & HOFFMANN, A. 2011. The specificity of innate immune responses is enforced by repression of interferon response elements by NF-kappaB p50. *Sci Signal,* 4**,** ra11.

764 CORZO, J. 2006. Time, the forgotten dimension of ligand binding teaching. *Biochem Mol*
765 *Biol Educ,* 34**,** 413-6.
766 COURTOIS, G. & GILMORE, T. D. 2006. Mutations in the NF-kappaB signaling
767 pathway: implications for human disease. *Oncogene,* 25**,** 6831-43.
768 CRAMER, P., LARSON, C. J., VERDINE, G. L. & MULLER, C. W. 1997. Structure of the
769 human NF-kappaB p52 homodimer-DNA complex at 2.1 A resolution. *EMBO J,*
770 16**,** 7078-90.
771 DARDEN, T., YORK, D. & PEDERSEN, L. 1993. Particle Mesh Ewald - an N.Log(N)
772 Method for Ewald Sums in Large Systems. *Journal of Chemical Physics,* 98**,**
773 10089-10092.
774 DONOVAN, B. T., CHEN, H., JIPA, C., BAI, L. & POIRIER, M. G. 2019. Dissociation rate
775 compensation mechanism for budding yeast pioneer transcription factors. *Elife,*
776 8.
777 EMSLEY, P. & COWTAN, K. 2004. Coot: model-building tools for molecular graphics.
778 *Acta Crystallogr D Biol Crystallogr,* 60**,** 2126-32.
779 EMSLEY, P., LOHKAMP, B., SCOTT, W. G. & COWTAN, K. 2010. Features and
780 development of Coot. *Acta Crystallogr D Biol Crystallogr,* 66**,** 486-501.
781 ESCALANTE, C. R., SHEN, L., THANOS, D. & AGGARWAL, A. K. 2002. Structure of
782 NF-kappaB p50/p65 heterodimer bound to the PRDII DNA element from the
783 interferon-beta promoter. *Structure,* 10**,** 383-91.
784 FUSCO, A. J., HUANG, D. B., MILLER, D., WANG, V. Y., VU, D. & GHOSH, G. 2009.
785 NF-kappaB p52:RelB heterodimer recognizes two classes of kappaB sites with
786 two distinct modes. *EMBO Rep,* 10**,** 152-9.
787 GARVIE, C. W. & WOLBERGER, C. 2001. Recognition of specific DNA sequences. *Mol*
788 *Cell,* 8**,** 937-46.
789 GHOSH, G., VAN DUYNE, G., GHOSH, S. & SIGLER, P. B. 1995. Structure of NF-
790 kappa B p50 homodimer bound to a kappa B site. *Nature,* 373**,** 303-10.
791 GHOSH, G., WANG, V. Y., HUANG, D. B. & FUSCO, A. 2012. NF-kappaB regulation:
792 lessons from structures. *Immunol Rev,* 246**,** 36-58.
793 GONZALEZ, P. A., CARRENO, L. J., COOMBS, D., MORA, J. E., PALMIERI, E.,
794 GOLDSTEIN, B., NATHENSON, S. G. & KALERGIS, A. M. 2005. T cell receptor
795 binding kinetics required for T cell activation depend on the density of cognate
796 ligand on the antigen-presenting cell. *Proc Natl Acad Sci U S A,* 102**,** 4824-9.
797 GROSS, A. W. & LODISH, H. F. 2006. Cellular trafficking and degradation of
798 erythropoietin and novel erythropoiesis stimulating protein (NESP). *J Biol Chem,*
799 281**,** 2024-32.
800 HAYASHI, M., NAKASHIMA, T., TANIGUCHI, M., KODAMA, T., KUMANOGOH, A. &
801 TAKAYANAGI, H. 2012. Osteoprotection by semaphorin 3A. *Nature,* 485**,** 69-74.
802 HESS, B., BEKKER, H., BERENDSEN, H. J. C. & FRAAIJE, J. G. E. M. 1997. LINCS: A
803 linear constraint solver for molecular simulations. *Journal of Computational*
804 *Chemistry,* 18**,** 1463-1472.
805 HOFFMANN, A., LEUNG, T. H. & BALTIMORE, D. 2003. Genetic analysis of NF-
806 kappaB/Rel transcription factors defines functional specificities. *Embo J,* 22**,**
807 5530-9.
808 HUANG, D. B., CHEN, Y. Q., RUETSCHE, M., PHELPS, C. B. & GHOSH, G. 2001. X-
809 ray crystal structure of proto-oncogene product c-Rel bound to the CD28
810 response element of IL-2. *Structure (Camb),* 9**,** 669-78.
811 HUANG, D. B., PHELPS, C. B., FUSCO, A. J. & GHOSH, G. 2005. Crystal structure of a
812 free kappaB DNA: insights into DNA recognition by transcription factor NF-
813 kappaB. *J Mol Biol,* 346**,** 147-60.

814 HUMPHREY, W., DALKE, A. & SCHULTEN, K. 1996. VMD: visual molecular dynamics.
815 *J Mol Graph,* 14**,** 33-8, 27-8.
816 JORGENSEN, W. L., CHANDRASEKHAR, J., MADURA, J. D., IMPEY, R. W. & KLEIN,
817 M. L. 1983. Comparison of Simple Potential Functions for Simulating Liquid
818 Water. *Journal of Chemical Physics,* 79**,** 926-935.
819 KEATS, J. J., FONSECA, R., CHESI, M., SCHOP, R., BAKER, A., CHNG, W. J., VAN
820 WIER, S., TIEDEMANN, R., SHI, C. X., SEBAG, M., BRAGGIO, E., HENRY, T.,
821 ZHU, Y. X., FOGLE, H., PRICE-TROSKA, T., AHMANN, G., MANCINI, C.,
822 BRENTS, L. A., KUMAR, S., GREIPP, P., DISPENZIERI, A., BRYANT, B.,
823 MULLIGAN, G., BRUHN, L., BARRETT, M., VALDEZ, R., TRENT, J.,
824 STEWART, A. K., CARPTEN, J. & BERGSAGEL, P. L. 2007. Promiscuous
825 mutations activate the noncanonical NF-kappaB pathway in multiple myeloma.
826 *Cancer Cell,* 12**,** 131-44.
827 KONTGEN, F., GRUMONT, R. J., STRASSER, A., METCALF, D., LI, R., TARLINTON,
828 D. & GERONDAKIS, S. 1995. Mice lacking the c-rel proto-oncogene exhibit
829 defects in lymphocyte proliferation, humoral immunity, and interleukin-2
830 expression. *Genes Dev,* 9**,** 1965-77.
831 LAVERY, R., MOAKHER, M., MADDOCKS, J. H., PETKEVICIUTE, D. &
832 ZAKRZEWSKA, K. 2009. Conformational analysis of nucleic acids revisited:
833 Curves+. *Nucleic Acids Res,* 37**,** 5917-29.
834 LENARDO, M. J. & BALTIMORE, D. 1989. NF-kappa B: a pleiotropic mediator of
835 inducible and tissue-specific gene control. *Cell,* 58**,** 227-9.
836 LEUNG, T. H., HOFFMANN, A. & BALTIMORE, D. 2004. One nucleotide in a kappaB
837 site can determine cofactor specificity for NF-kappaB dimers. *Cell,* 118**,** 453-64.
838 LIM, C. A., YAO, F., WONG, J. J., GEORGE, J., XU, H., CHIU, K. P., SUNG, W. K.,
839 LIPOVICH, L., VEGA, V. B., CHEN, J., SHAHAB, A., ZHAO, X. D., HIBBERD,
840 M., WEI, C. L., LIM, B., NG, H. H., RUAN, Y. & CHIN, K. C. 2007. Genome-wide
841 mapping of RELA(p65) binding identifies E2F1 as a transcriptional activator
842 recruited by NF-kappaB upon TLR4 activation. *Mol Cell,* 27**,** 622-35.
843 LINDAHL, E., ABRAHAM, M., HESS, B. & SPOEL, D. V. D. 2020. GROMACS 2020.6
844 Manual.
845 MAIER, J. A., MARTINEZ, C., KASAVAJHALA, K., WICKSTROM, L., HAUSER, K. E. &
846 SIMMERLING, C. 2015. ff14SB: Improving the Accuracy of Protein Side Chain
847 and Backbone Parameters from ff99SB. *Journal of Chemical Theory and*
848 *Computation,* 11**,** 3696-3713.
849 MARKGREN, P. O., SCHAAL, W., HAMALAINEN, M., KARLEN, A., HALLBERG, A.,
850 SAMUELSSON, B. & DANIELSON, U. H. 2002. Relationships between structure
851 and interaction kinetics for HIV-1 protease inhibitors. *J Med Chem,* 45**,** 5430-9.
852 MARTONE, R., EUSKIRCHEN, G., BERTONE, P., HARTMAN, S., ROYCE, T. E.,
853 LUSCOMBE, N. M., RINN, J. L., NELSON, F. K., MILLER, P., GERSTEIN, M.,
854 WEISSMAN, S. & SNYDER, M. 2003. Distribution of NF-kappaB-binding sites
855 across human chromosome 22. *Proc Natl Acad Sci U S A,* 100**,** 12247-52.
856 MCCOY, A. J., GROSSE-KUNSTLEVE, R. W., ADAMS, P. D., WINN, M. D., STORONI,
857 L. C. & READ, R. J. 2007. Phaser crystallographic software. *J Appl Crystallogr,*
858 40**,** 658-674.
859 MOORTHY, A. K., HUANG, D. B., WANG, V. Y., VU, D. & GHOSH, G. 2007. X-ray
860 Structure of a NF-kappaB p50/RelB/DNA Complex Reveals Assembly of Multiple
861 Dimers on Tandem kappaB Sites. *J Mol Biol*.
862 MULERO, M. C., SHAHABI, S., KO, M. S., SCHIFFER, J. M., HUANG, D. B., WANG, V.
863 Y., AMARO, R. E., HUXFORD, T. & GHOSH, G. 2018. Protein Cofactors Are

Essential for High-Affinity DNA Binding by the Nuclear Factor kappaB RelA Subunit. *Biochemistry,* 57**,** 2943-2957.

MULERO, M. C., WANG, V. Y., HUXFORD, T. & GHOSH, G. 2019. Genome reading by the NF-kappaB transcription factors. *Nucleic Acids Res,* 47**,** 9967-9989.

MULLER, C. W., REY, F. A., SODEOKA, M., VERDINE, G. L. & HARRISON, S. C. 1995. Structure of the NF-kappa B p50 homodimer bound to DNA. *Nature,* 373**,** 311-7.

MURSHUDOV, G. N., SKUBAK, P., LEBEDEV, A. A., PANNU, N. S., STEINER, R. A., NICHOLLS, R. A., WINN, M. D., LONG, F. & VAGIN, A. A. 2011. REFMAC5 for the refinement of macromolecular crystal structures. *Acta Crystallogr D Biol Crystallogr,* 67**,** 355-67.

NAKAJIMA, H., KIYOKAWA, N., KATAGIRI, Y. U., TAGUCHI, T., SUZUKI, T., SEKINO, T., MIMORI, K., EBATA, T., SAITO, M., NAKAO, H., TAKEDA, T. & FUJIMOTO, J. 2001. Kinetic analysis of binding between Shiga toxin and receptor glycolipid Gb3Cer by surface plasmon resonance. *J Biol Chem,* 276**,** 42915-22.

NATOLI, G., SACCANI, S., BOSISIO, D. & MARAZZI, I. 2005. Interactions of NF-kappaB with chromatin: the art of being at the right place at the right time. *Nat Immunol,* 6**,** 439-45.

PAN, J. & MCEVER, R. P. 1995. Regulation of the human P-selectin promoter by Bcl-3 and specific homodimeric members of the NF-kappa B/Rel family. *J Biol Chem,* 270**,** 23077-83.

PANNE, D., MANIATIS, T. & HARRISON, S. C. 2007. An atomic model of the interferon-beta enhanceosome. *Cell,* 129**,** 1111-23.

SCHRODINGER, LLC 2015. The PyMOL Molecular Graphics System, Version 2.0.

SEKIYA, T., MUTHURAJAN, U. M., LUGER, K., TULIN, A. V. & ZARET, K. S. 2009. Nucleosome-binding affinity as a primary determinant of the nuclear mobility of the pioneer transcription factor FoxA. *Genes Dev,* 23**,** 804-9.

SIGGERS, T., CHANG, A. B., TEIXEIRA, A., WONG, D., WILLIAMS, K. J., AHMED, B., RAGOUSSIS, J., UDALOVA, I. A., SMALE, S. T. & BULYK, M. L. 2011. Principles of dimer-specific gene regulation revealed by a comprehensive characterization of NF-kappaB family DNA binding. *Nat Immunol,* 13**,** 95-102.

WANG, V. Y., HUANG, W., ASAGIRI, M., SPANN, N., HOFFMANN, A., GLASS, C. & GHOSH, G. 2012. The transcriptional specificity of NF-kappaB dimers is coded within the kappaB DNA response elements. *Cell Rep,* 2**,** 824-39.

WANG, V. Y., LI, Y., KIM, D., ZHONG, X., DU, Q., GHASSEMIAN, M. & GHOSH, G. 2017. Bcl3 Phosphorylation by Akt, Erk2, and IKK Is Required for Its Transcriptional Activity. *Mol Cell,* 67**,** 484-497 e5.

ZGARBOVÁ, M., ŠPONER, J., OTYEPKA, M., CHEATHAM, T. E., GALINDO-MURILLO, R. & JUREČKA, P. 2015. Refinement of the Sugar–Phosphate Backbone Torsion Beta for AMBER Force Fields Improves the Description of Z- and B-DNA. *Journal of Chemical Theory and Computation,* 11**,** 5723-5736.

ZHANG, Q., LENARDO, M. J. & BALTIMORE, D. 2017. 30 Years of NF-kappaB: A Blossoming of Relevance to Human Pathobiology. *Cell,* 168**,** 37-57.

ZHAO, B., BARRERA, L. A., ERSING, I., WILLOX, B., SCHMIDT, S. C., GREENFELD, H., ZHOU, H., MOLLO, S. B., SHI, T. T., TAKASAKI, K., JIANG, S., CAHIR-MCFARLAND, E., KELLIS, M., BULYK, M. L., KIEFF, E. & GEWURZ, B. E. 2014. The NF-kappaB genomic landscape in lymphoblastoid B cells. *Cell Rep,* 8**,** 1595-606.

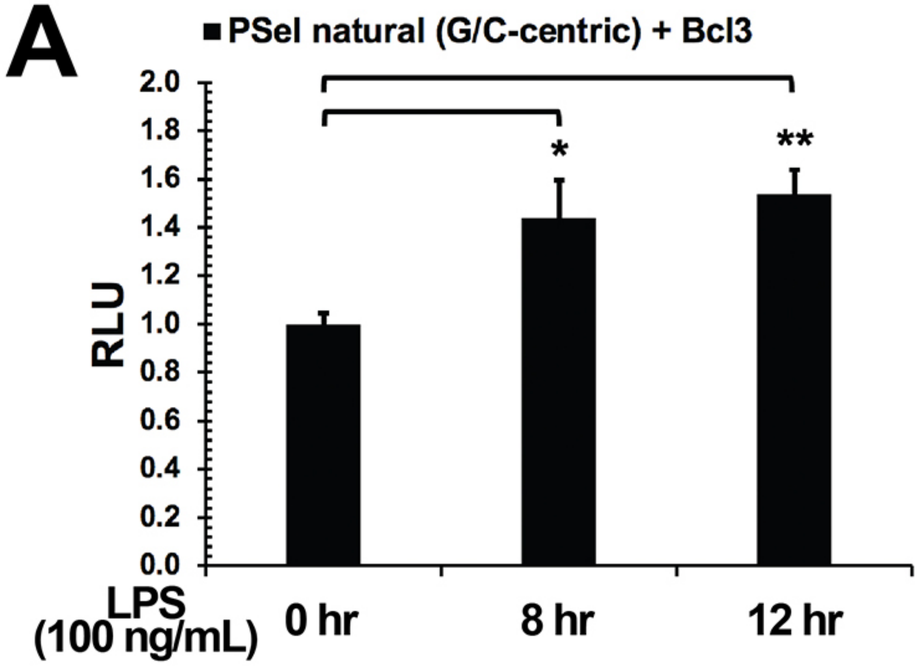

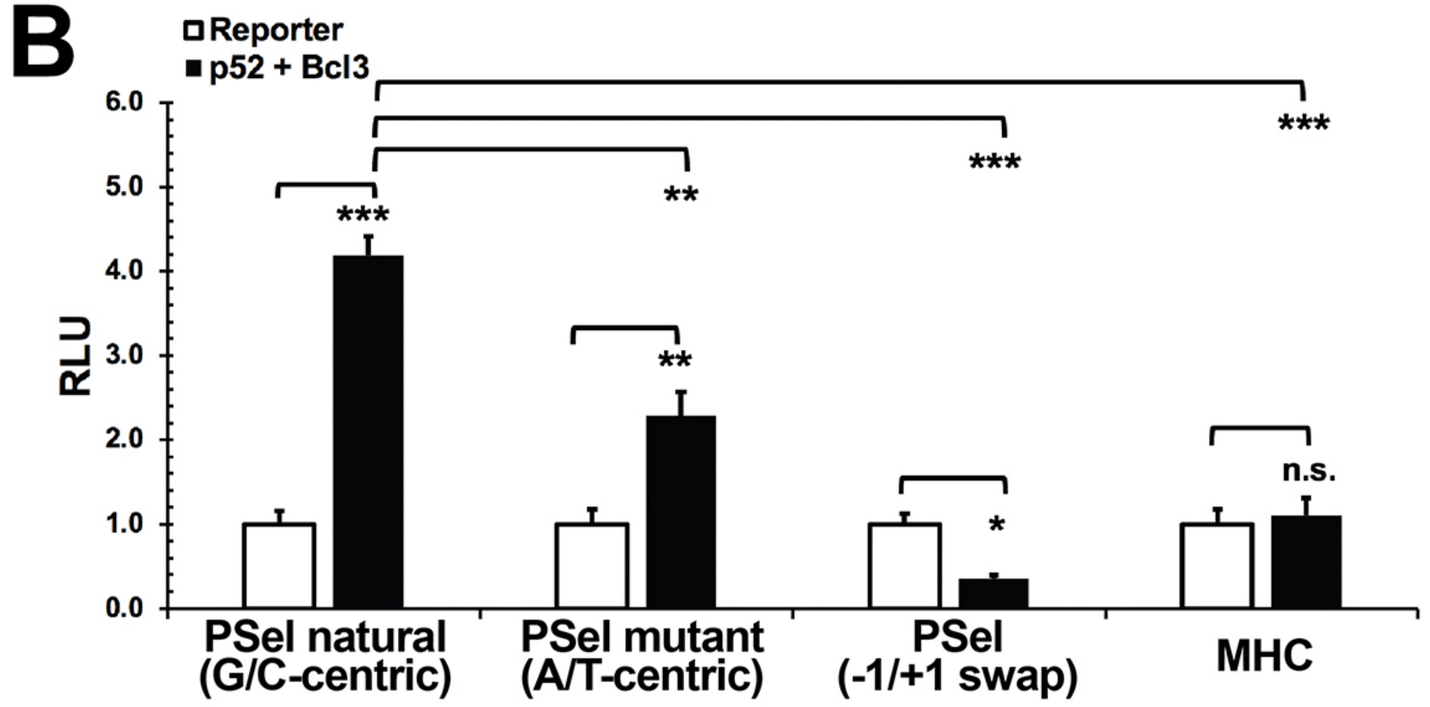

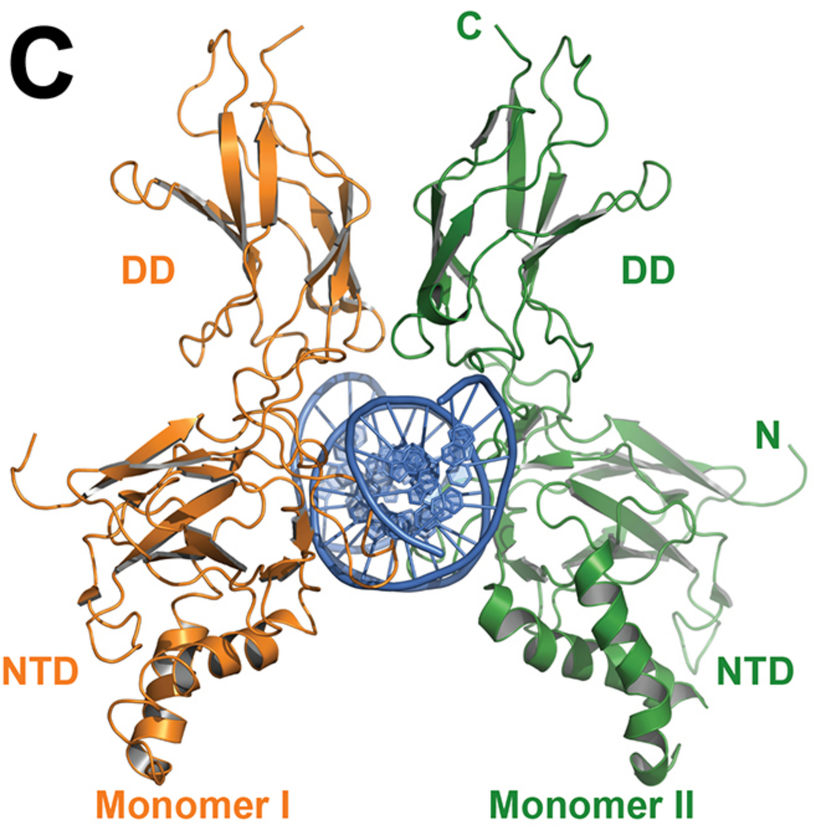

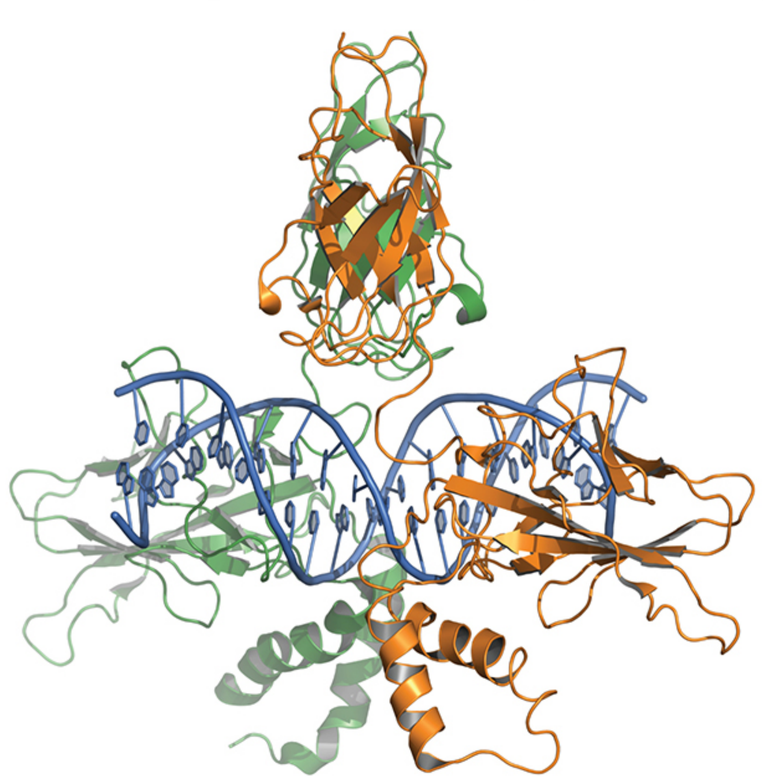

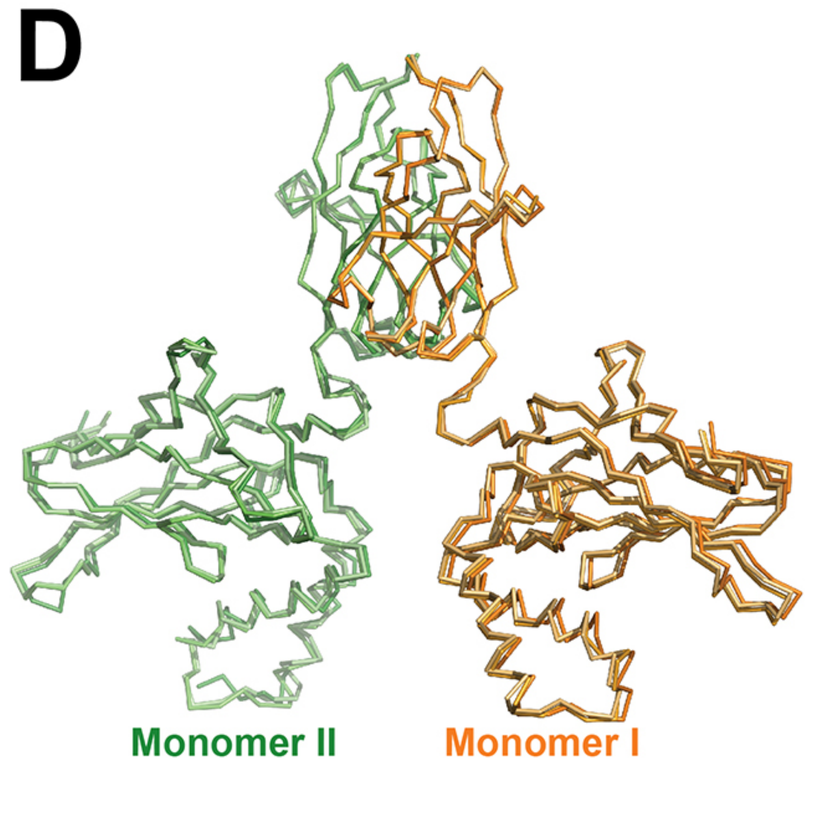

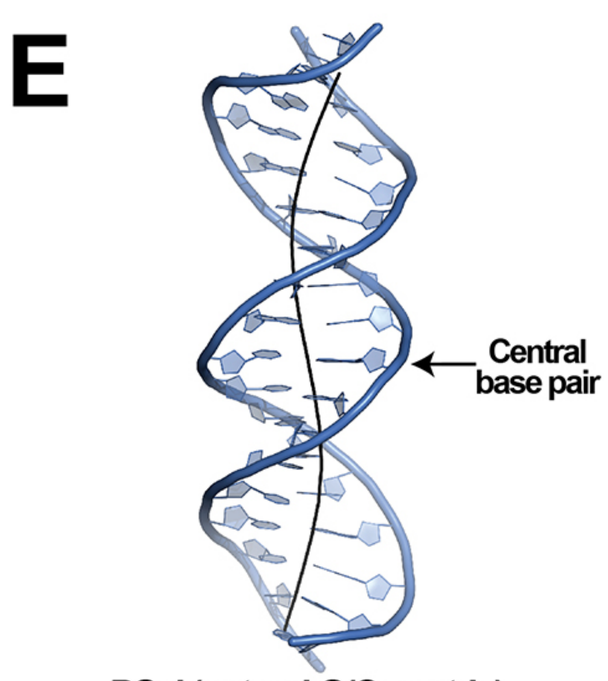

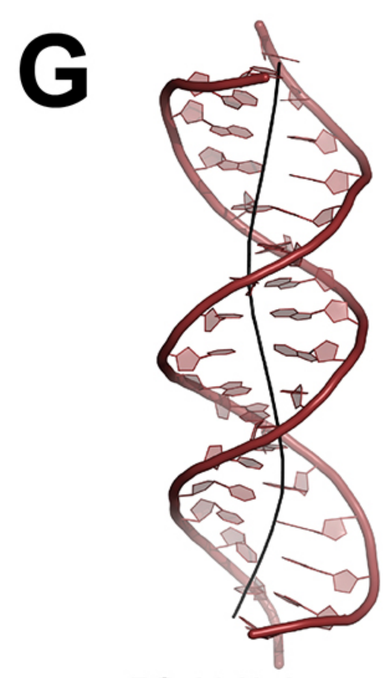

PSel (natural G/C-centric) κB DNA

-5 -4 -3 -2 -1 0 +1 +2 +3 +4 +5

5′-GAAG**GGGGT**G**ACCCC**TTG-3′

3′-CTTC**CCCCA**C**TGGGG**AAC-5′

PSel (mutant A/T-centric) κB DNA

-5 -4 -3 -2 -1 0 +1 +2 +3 +4 +5

5′-GAAG**GGGGT**A**ACCCC**TTG-3′

3′-CTTC**CCCCA**T**TGGGG**AAC-5′

PSel (-1/+1 swap) κB DNA

-5 -4 -3 -2 -1 0 +1 +2 +3 +4 +5

5′-GAAG**GGGGA**G**TCCCC**TTG-3′

3′-CTTC**CCCCT**C**AGGGG**AAC-5′

		PSel (natural G/C-centric) κB DNA *(this study)*		PSel (-1/+1 swap) κB DNA *(this study)*		PSel (mutant A/T-centric) κB DNA *(this study)*				MHC κB DNA		κB-33				κB-55				Ideal B-DNA
Protein		p52(1 - 398)		p52(1 - 398)		p52(1 - 398)		p52(1 - 327)		p52(35 - 329)		free		RelA:RelA bound		free		p52:RelB bound		
DNA length		18 bp		18 bp		18 bp		13 bp		13 bp										
		Minor groove width	Major groove depth	Minor groove width	Major groove depth	Minor groove width	Major groove depth	Minor groove width	Major groove depth	Minor groove width	Major groove depth	Minor groove width		Minor groove width		Minor groove width		Minor groove width		Minor groove width
Positions		A		A		A						C								
		G	6.7 / 6.8	G	7.5 / 7.4	G	7.9 / 7.4					T	7.1 / 6.7	6.6 / 6.0						
	- 5	G	6.4 / 6.0	G	6.8 / 6.1	G	6.6 / 6.1	G				G	6.5 / 5.5	5.6 / 5.3						
	- 4	G	5.9 / 5.7	G	5.6 / 5.9	G	5.9 / 5.6	G	7.3 /	G		G	6.3 / 6.4	5.2 / 4.1	G					
	- 3	G	5.8 / 5.8	G	6.3 / 6.0	G	5.8 / 5.5	G	7.4 / 6.0	G	5.5 /	A	6.0 / 4.6	3.1 / 2.8	G					5.9
	- 2	G	5.9 / 5.9	G	5.5 / 5.6	G	5.3 / 5.5	G	4.2 / 3.3	4.2 / 5.1	G	4.1 / 3.2	3.7 / 4.9	A	3.4 / 3.4	3.2 / 3.3	G	7.8 / 5.9	3.3	5.9	5.9
	- 1	T	6.5 / 7.7	5.7 / 6.7	A	6.3 / 7.5	6.2 / 6.8	T	6.3 / 7.4	6.1 / 6.8	T	3.1 / 3.6	5.3 / 5.0	A	3.0 / 3.5	5.4 / 5.7	A	3.7 / 3.7	3.6 / 4.1	A	4.4 / 3.9	3.2 / 3.7	5.9 / 5.9
	0	G	8.2 / 7.3	7.0 / 6.9	G	8.1 / 7.3	6.8 / 6.4	A	8.0 / 7.1	7.1 / 6.7	A	4.0 / 3.5	4.4 / 4.9	T	4.0 / 3.8	5.5 / 5.9	T	3.7 / 3.4	4.2 / 3.6	A	4.2 / 4.1	4.2 / 3.9	5.9 / 5.9
	+1	A	5.9 / 5.2	5.9 / 4.9	T	6.0 / 5.3	5.9 / 5.2	A	5.7 / 4.7	6.0 / 5.1	A	3.0 / 3.3	5.3 / 5.3	T	3.4 / 3.3	5.7 / 5.0	T	3.4 / 4.6	3.1 / 3.6	T	4.2 / 3.9	3.6 / 3.4	5.9 / 5.9
	+2	C	5.0 / 5.0	5.1 /	C	5.3 / 5.9	4.9 /	C	4.4 / 4.8	4.7 /	C	4.3 / 6.1	4.5 /	C	3.7 / 5.3	3.9 /	T	6.0 / 6.4	4.5 / 5.5	T	4.4 / 5.9		5.9 / 5.9
	+3	C	5.3 / 6.2	/	C	6.4 / 6.2	/	C	5.4 / 5.8	/	C	7.4 / 7.3	/	C			C	6.3 / 5.5	6.5 / 6.6	C	7.8		
	+4	C	7.1 / 7.3	/	C	6.2 / 6.8	/	C	6.5 / 6.9	/	C			C			C	6.5 / 6.7	6.6 / 6.9	C			
	+5	C	7.7 / 8.4	/	C	7.4 / 8.1	/	C	7.5 / 8.3	/	C						A	7.1	7.0				
		T	8.8	/	T	8.3	/	T	8.7	/							G						
		T			T			T									C						

A

- p52:p52 (1-398) bound to PSel (G/C-centric) [PDB 7CLI *(this study)*]
- p52:p52 (35-329) bound to MHC [PDB 1A3Q]

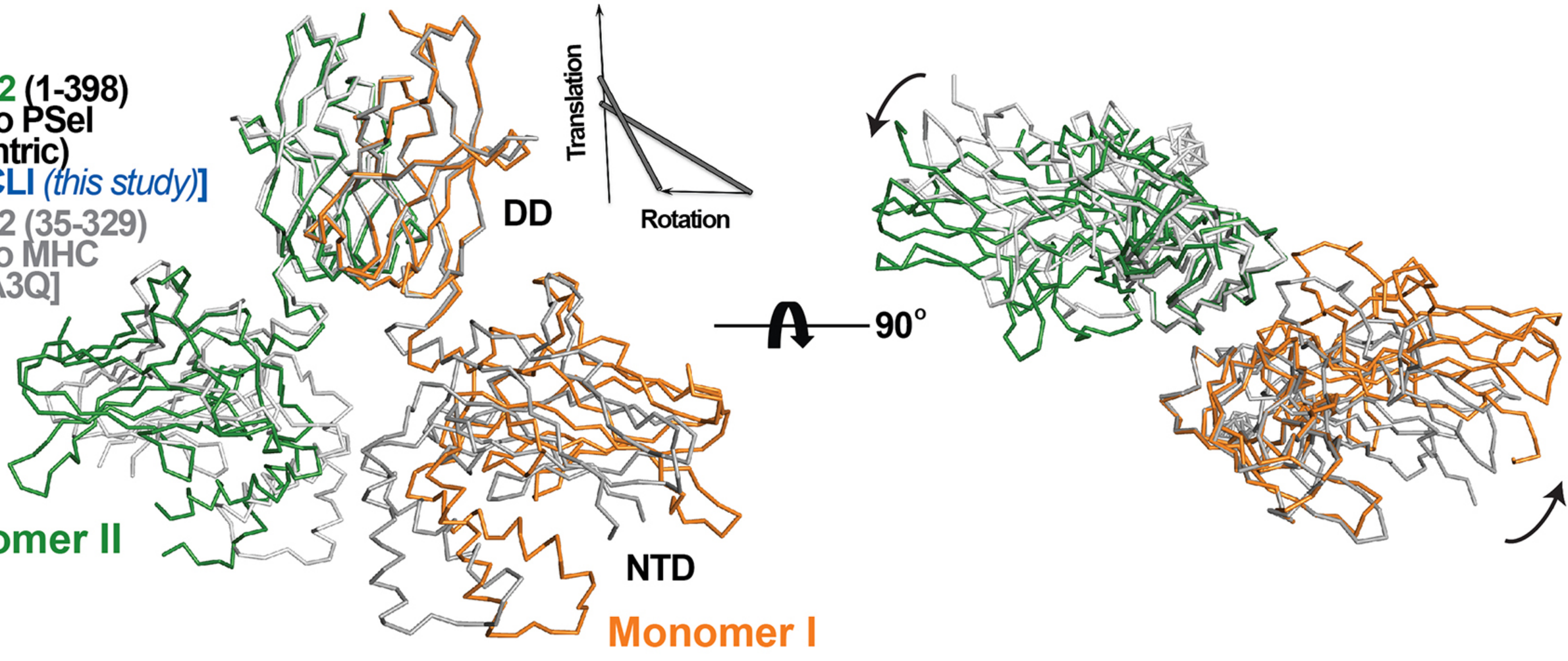

B

- p52:p52 (1-327) bound to PSel (A/T-centric) [PDB 7W7L *(this study)*]
- p52:p52 (35-329) bound to MHC [PDB 1A3Q]

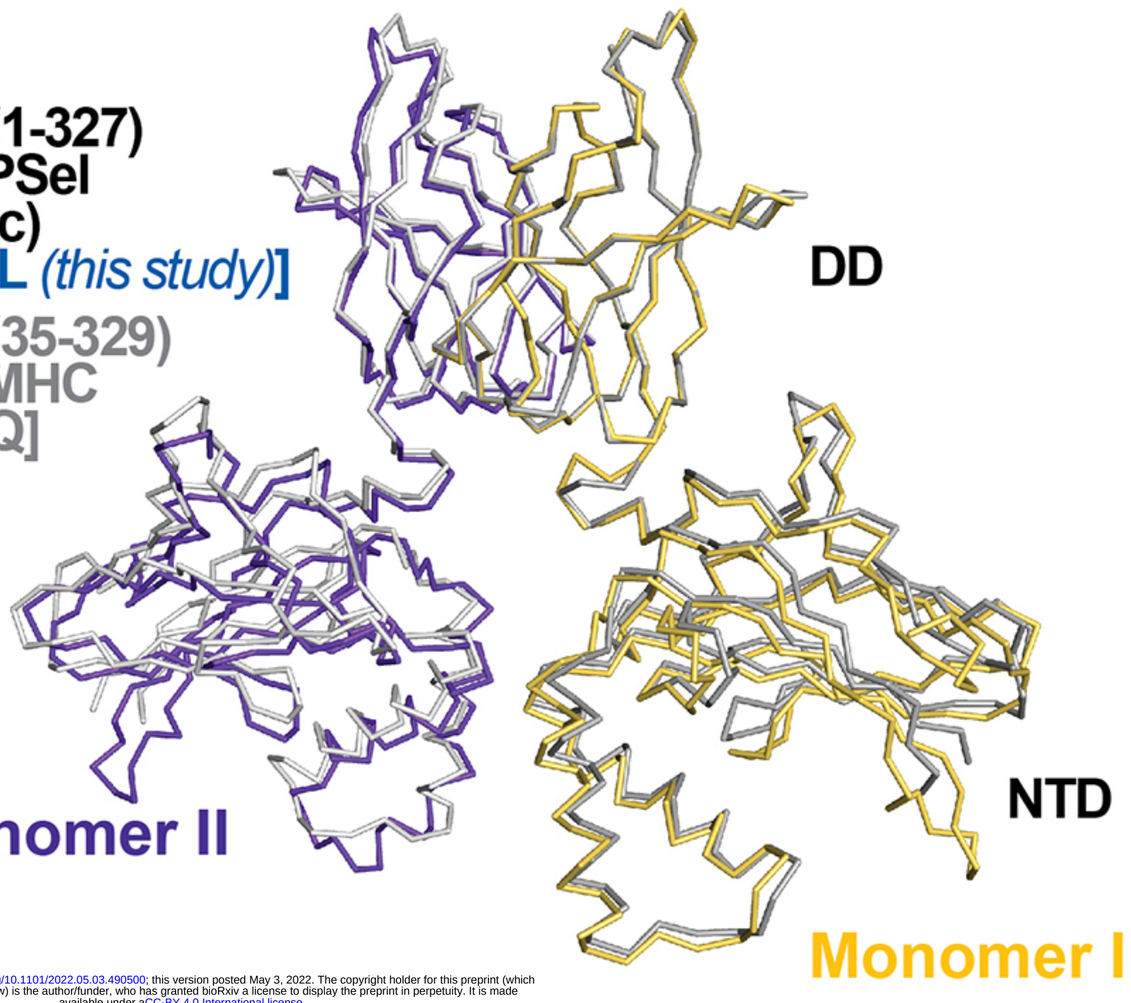

C

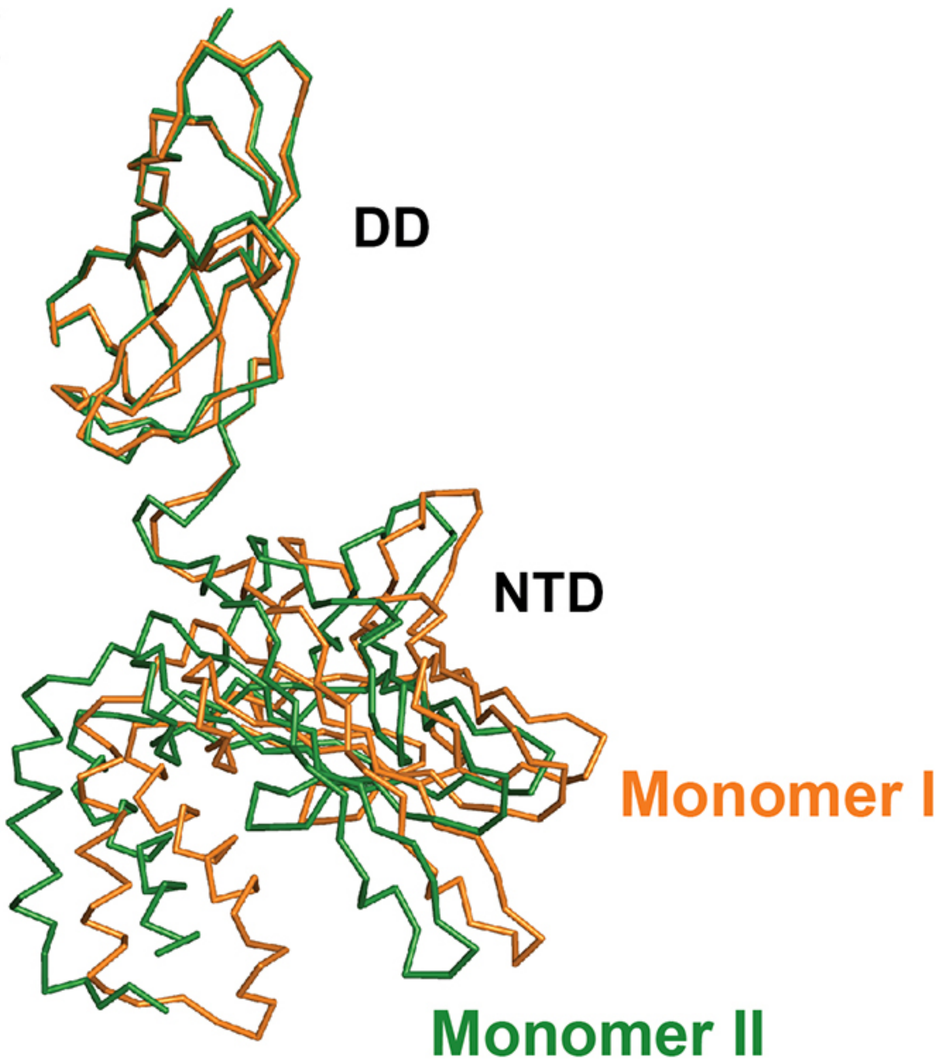

D

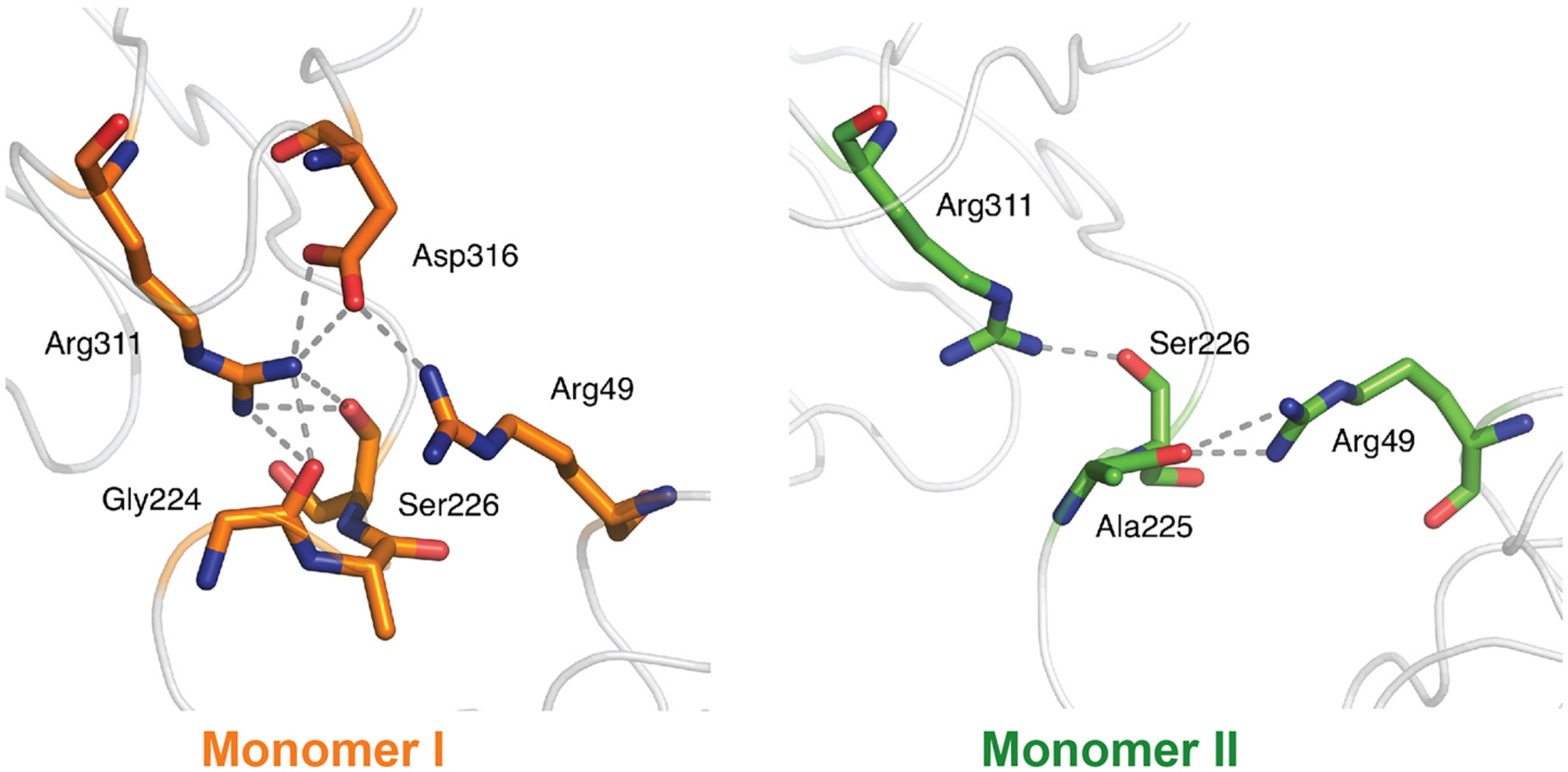

A

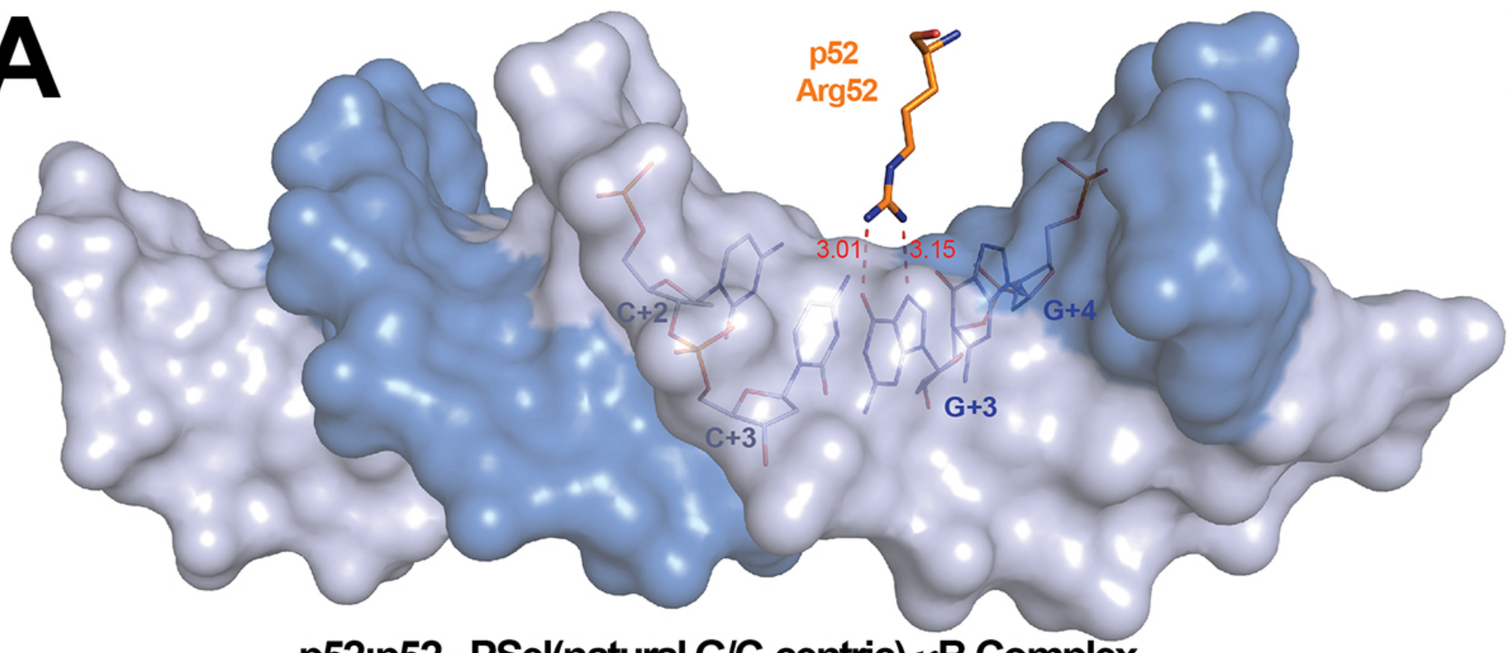

p52:p52 - PSel(natural G/C-centric)-κB Complex
(this study)

B

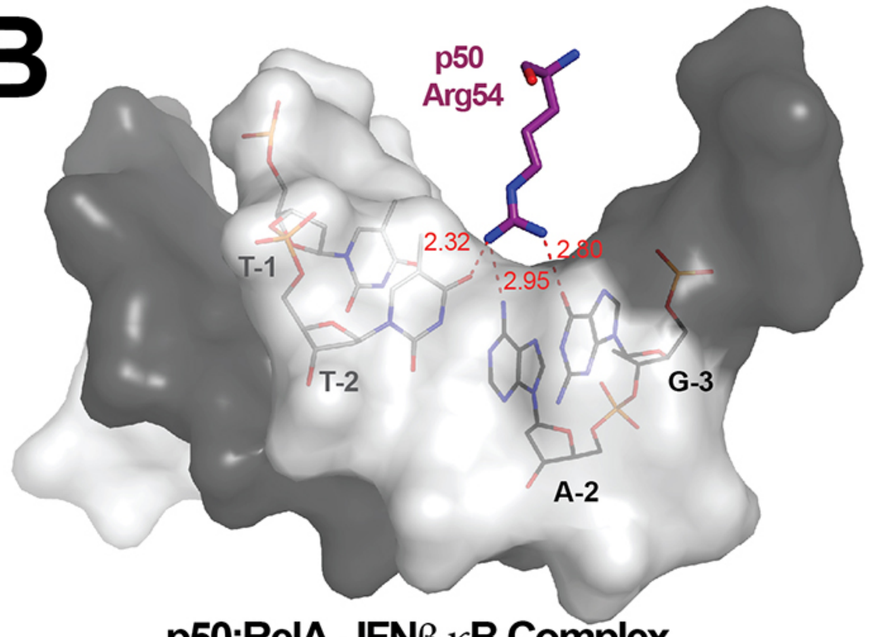

p50:RelA - IFNβ-κB Complex

C

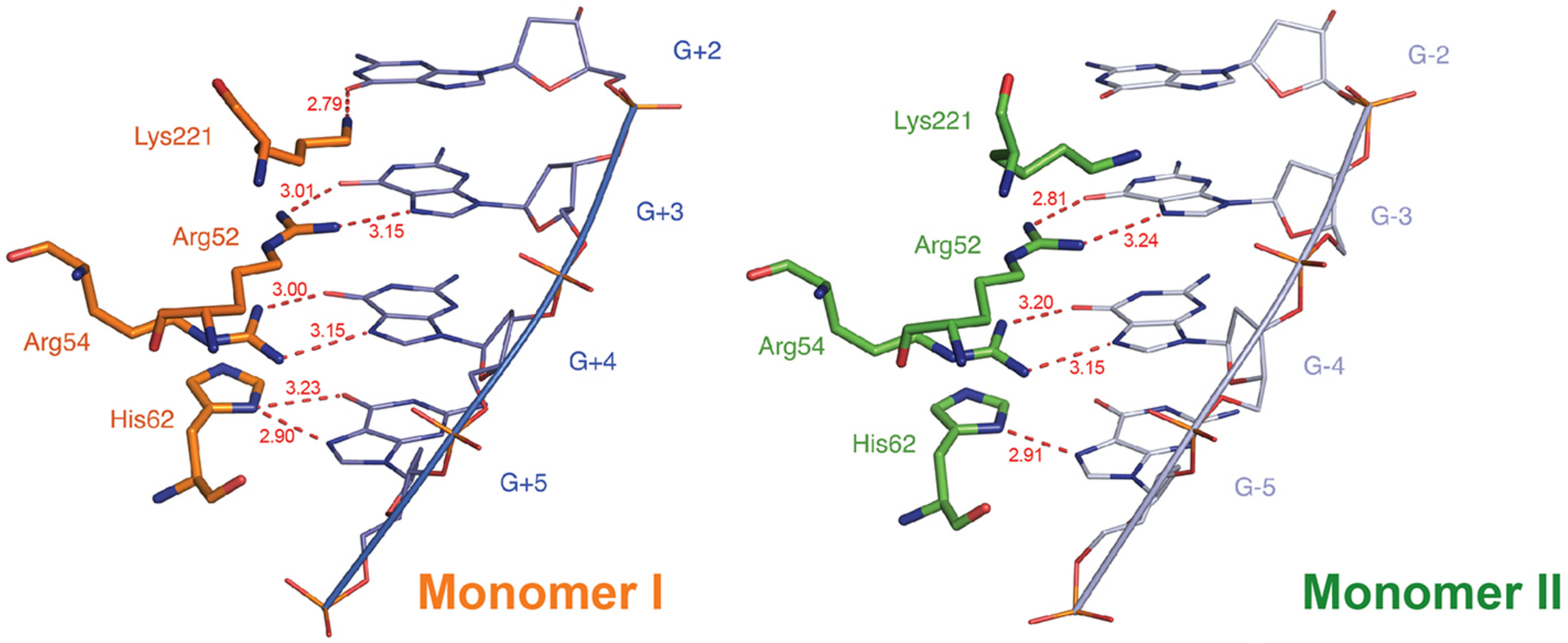

D

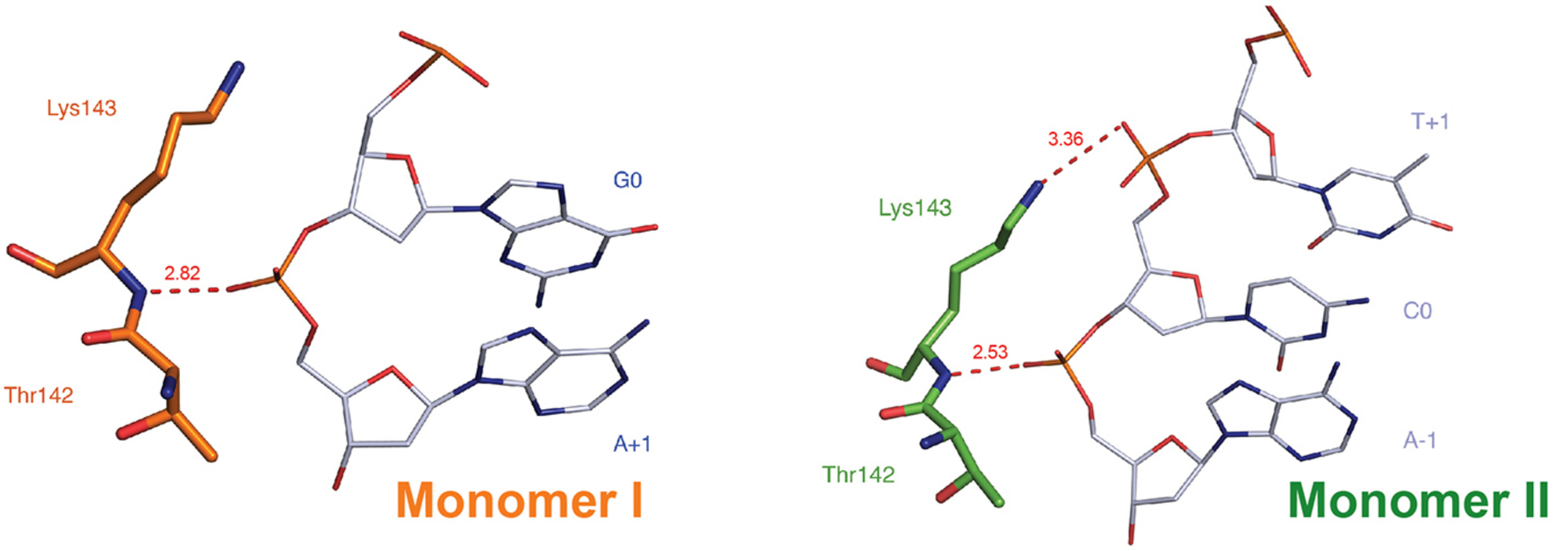

E

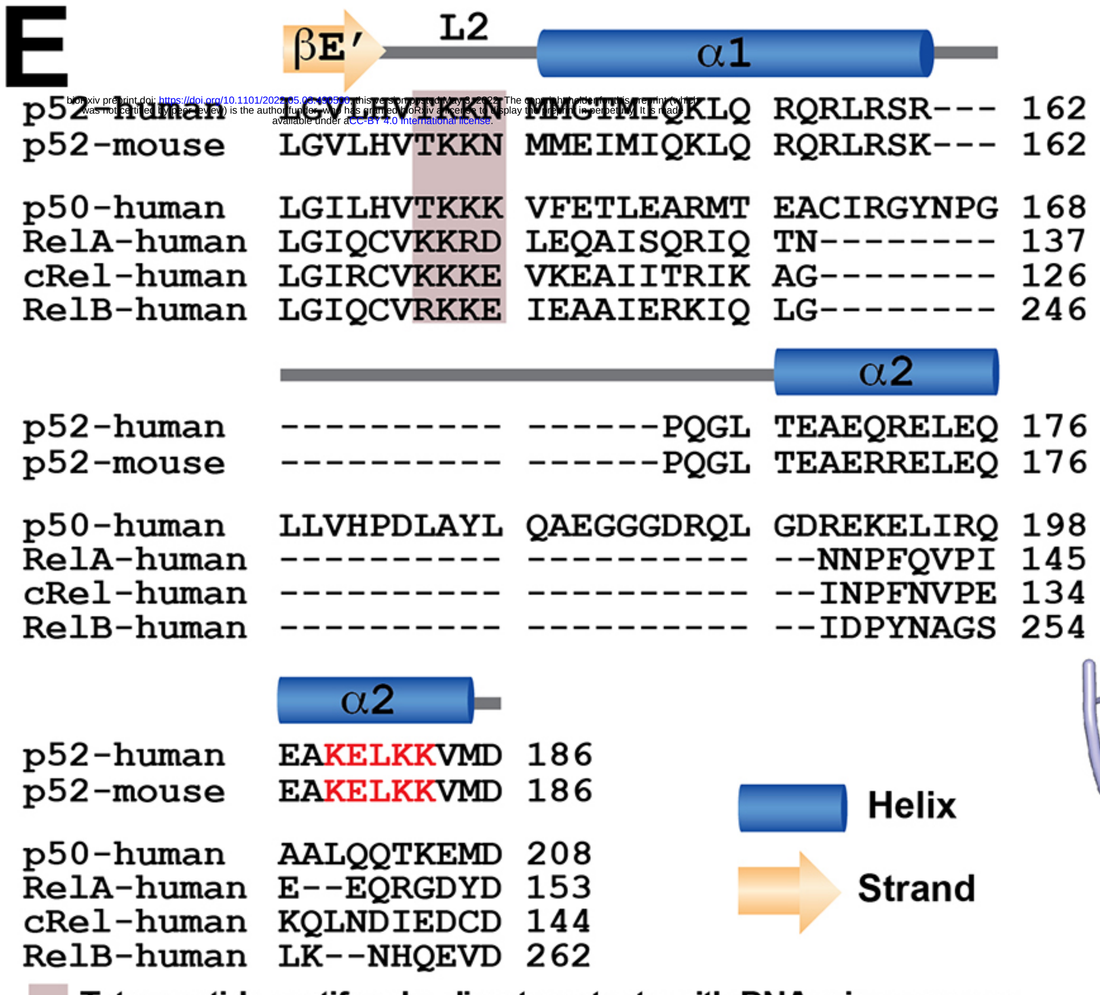

Tetrapeptide motif make direct contacts with DNA minor groove

XX Unique basic segment in p52

F

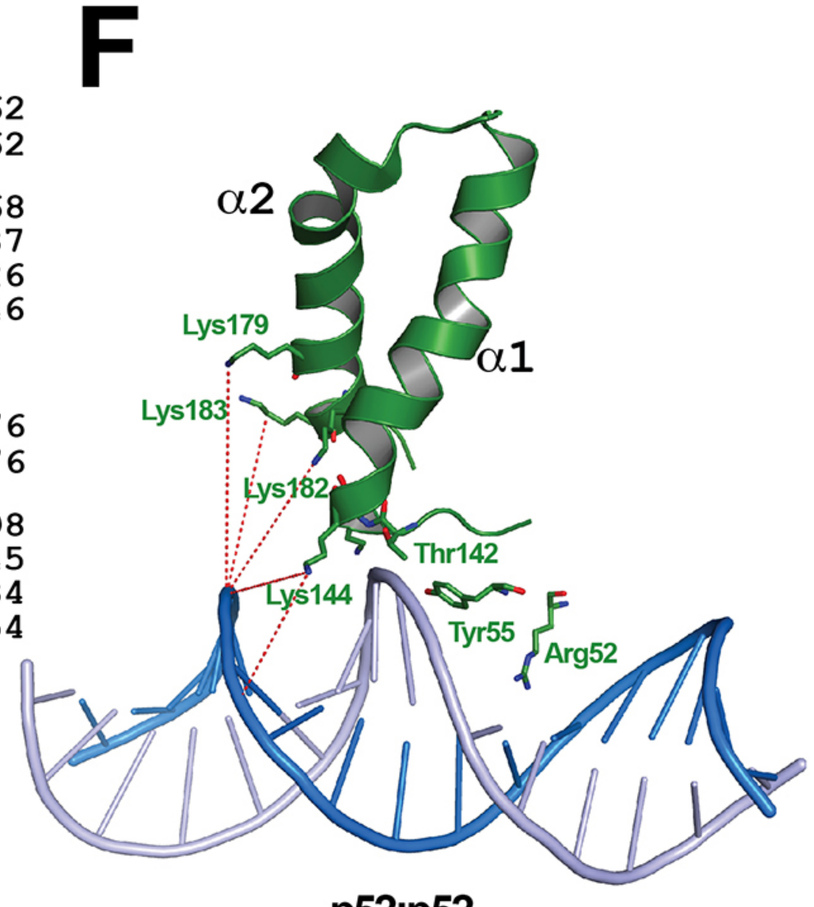

p52:p52 -
PSel(natural G/C-centric)-κB Complex
(this study)

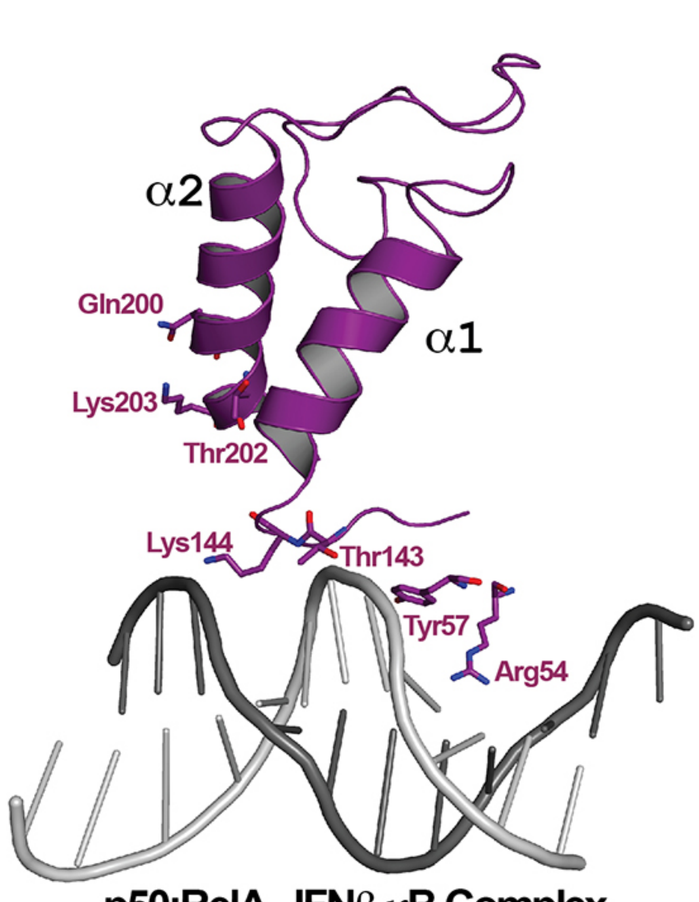

p50:RelA - IFNβ-κB Complex

A

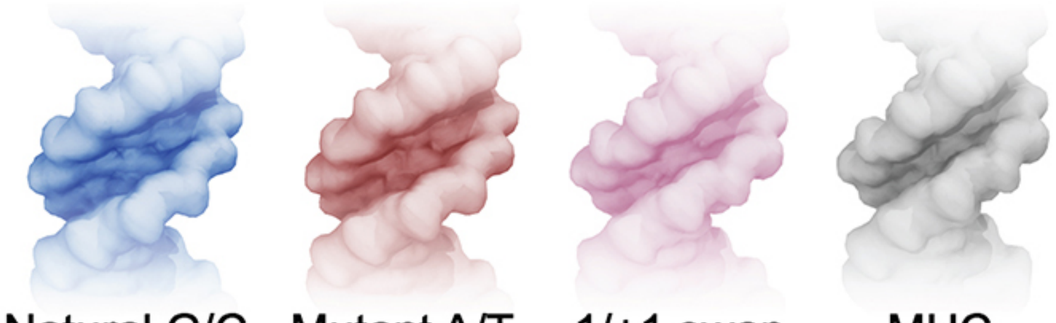

Natural G/C Mutant A/T -1/+1 swap MHC

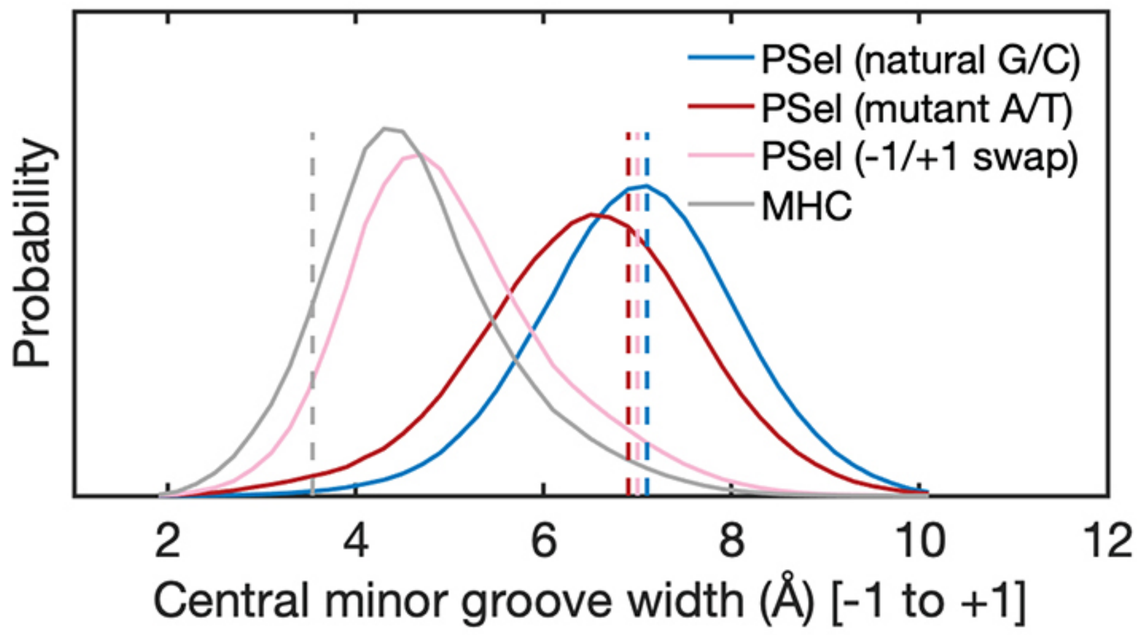

B

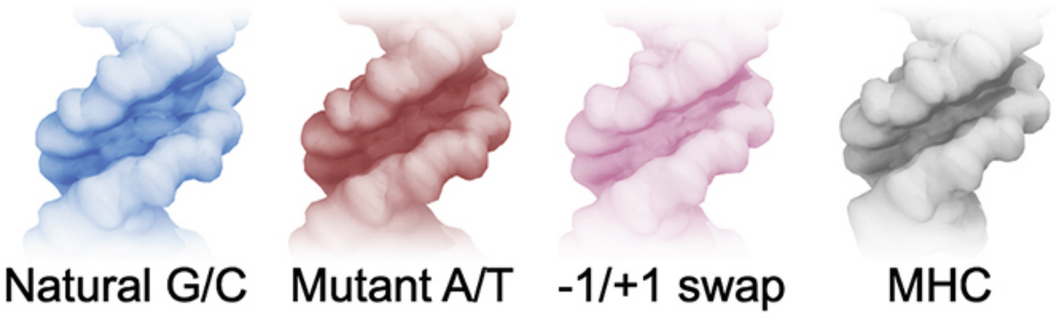

Natural G/C Mutant A/T -1/+1 swap MHC

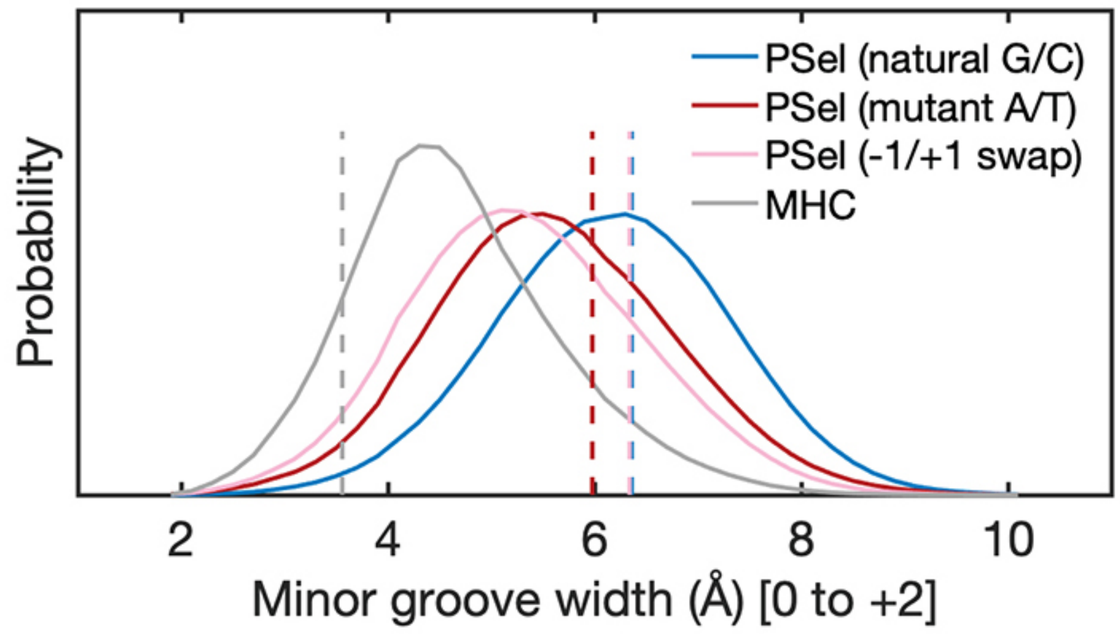

C

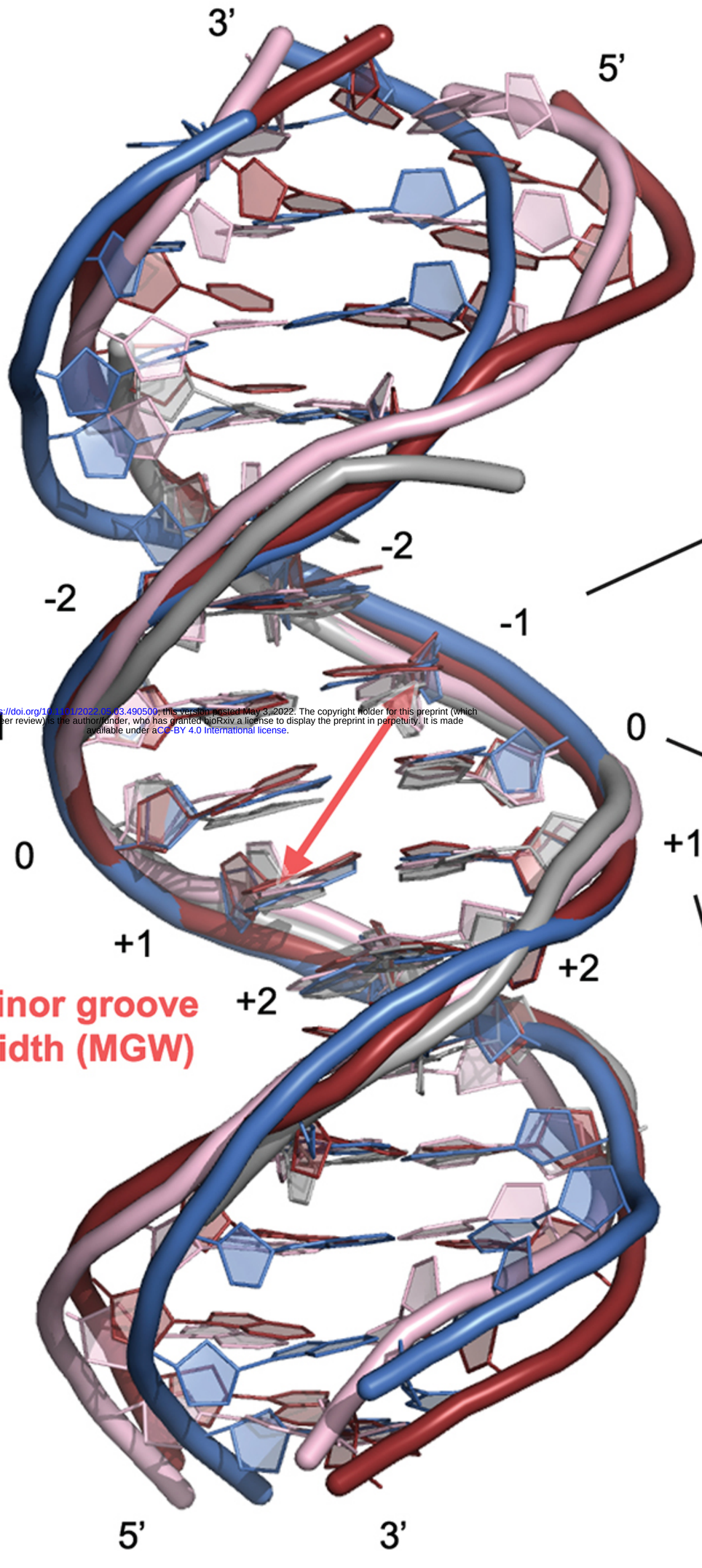

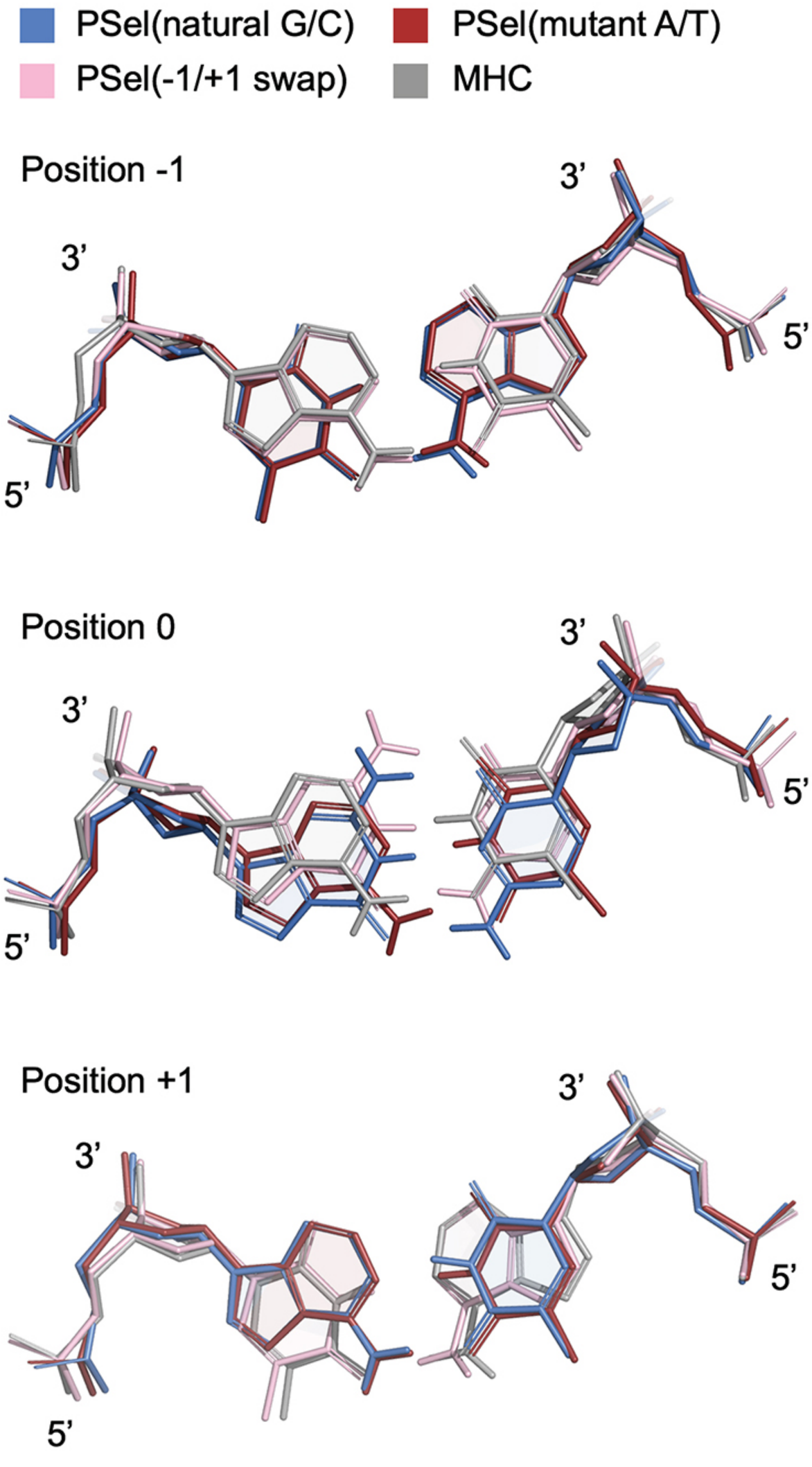

A

p52:p52-PSel (natural G/C-centric)

−5 −4 −3 −2 −1 0 +1 +2 +3 +4 +5

5′-GGAAG**GGGGTGACCCC**TTGG-3′

3′-CCTTC**CCCCACTGGGG**AACC-5′

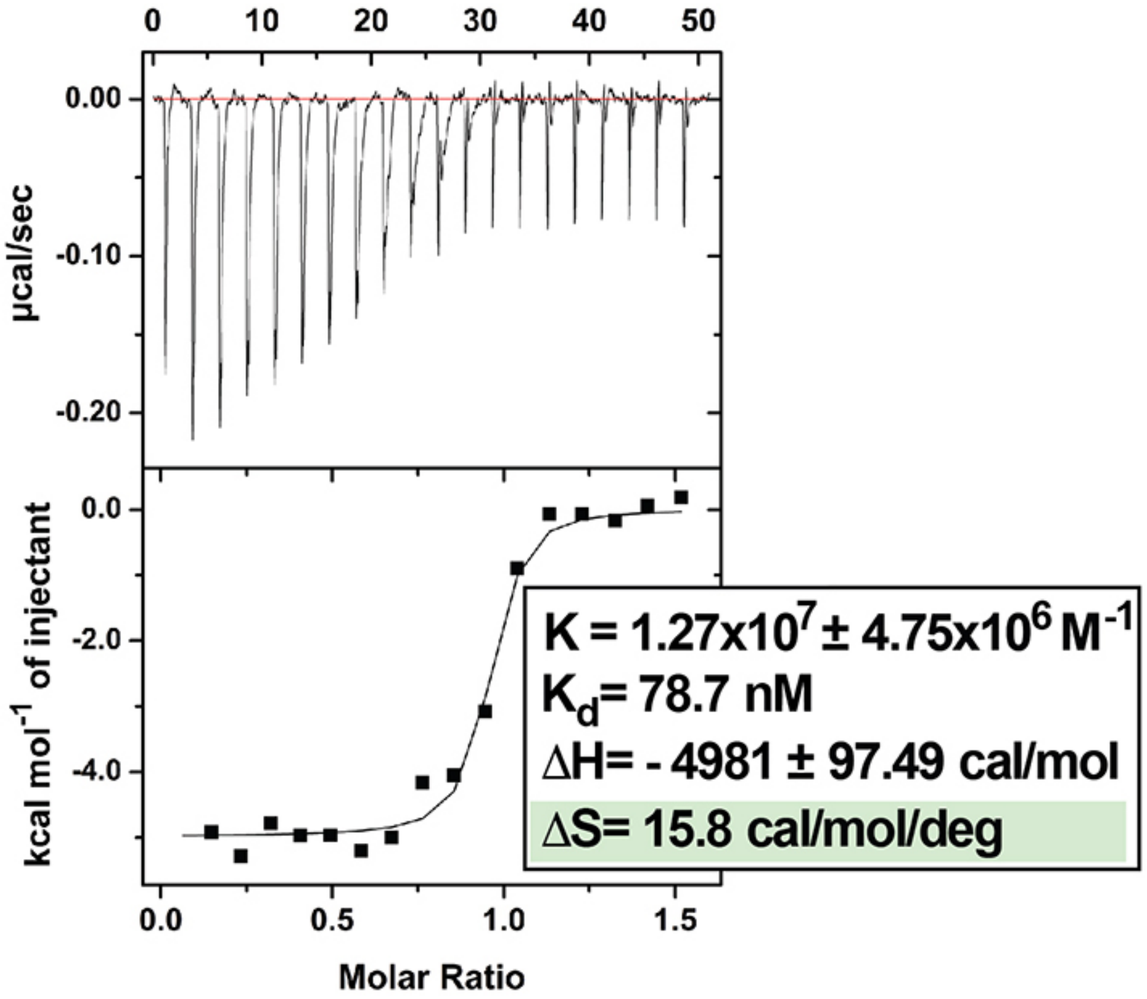

B

p52:p52-PSel (mutant A/T-centric)

−5 −4 −3 −2 −1 0 +1 +2 +3 +4 +5

5′-GGAAG**GGGGTAACCCC**TTGG-3′

3′-CCTTC**CCCCATTGGGG**AACC-5′

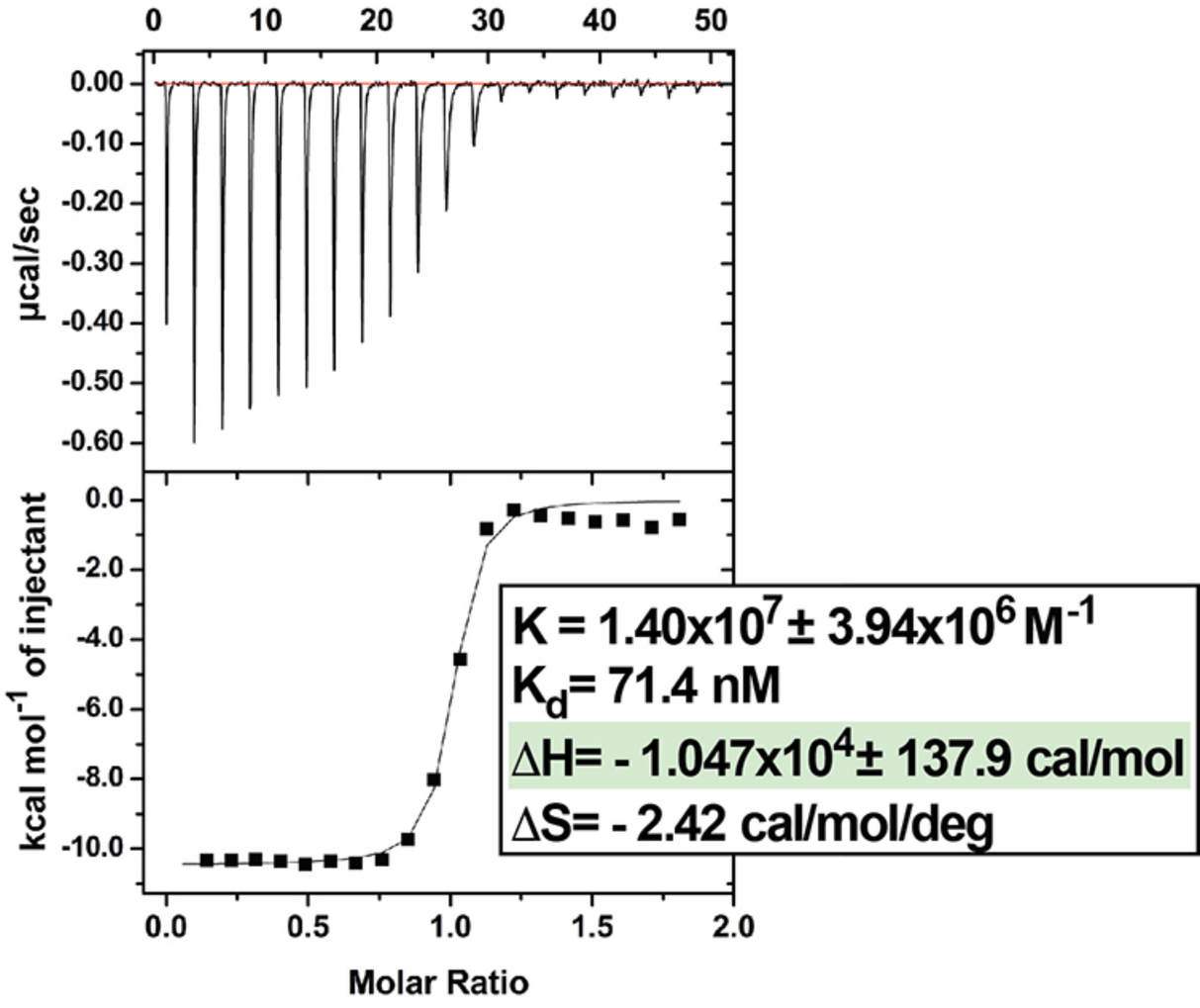

C

p52:p52-PSel (-1 A>T)

−5 −4 −3 −2 −1 0 +1 +2 +3 +4 +5

5′-GGAAG**GGGGAGTCCCC**TTGG-3′

3′-CCTTC**CCCCTCAGGGG**AACG-5′

D

p52:p52-MHC (natural A/T-centric)

−5 −4 −3 −2 −1 0 +1 +2 +3 +4 +5

5′-GGAAG**GGGGATTCCCC**TTGG-3′

3′-CCTTC**CCCCTAAGGGG**AACG-5′

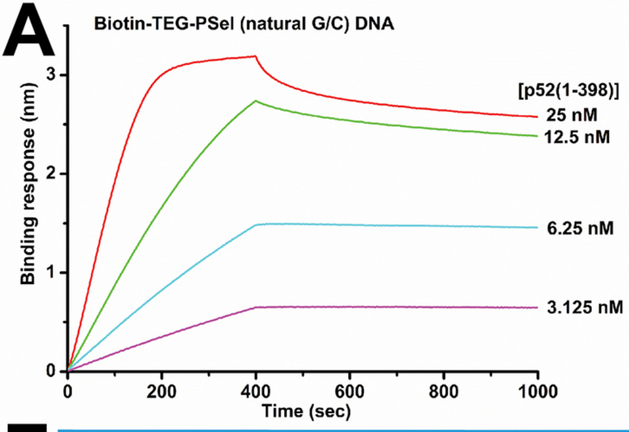

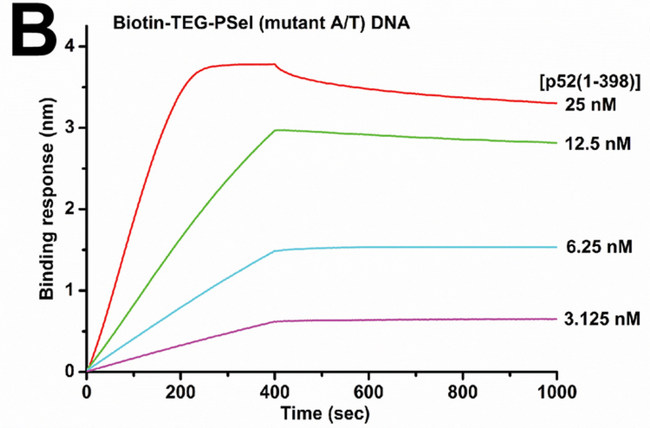

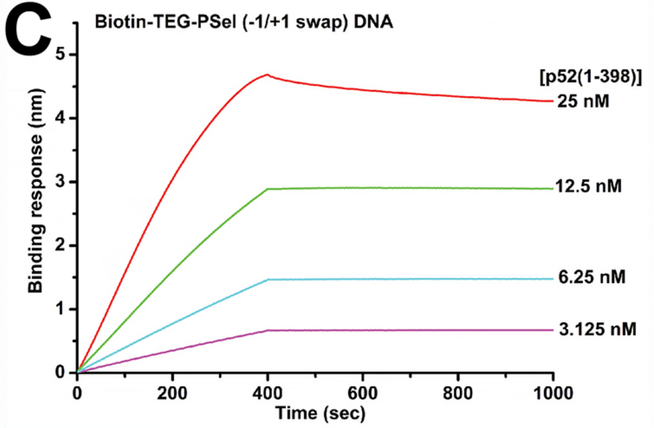

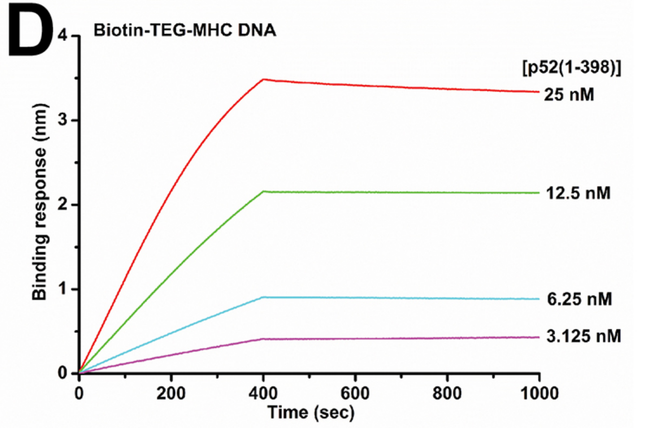

E **Kinetic analysis of p52:p52 homodimer binding to various κB DNAs by BLI**

	PSel(natual G/C-centric)	PSel(mutant A/T-centric)	PSel(-1/+1 swap)	MHC
K_d (nM)	0.95 ± 0.019 (0.86 ± 0.022)	0.90 ± 0.037 (0.69 ± 0.027)	0.66 ± 0.03 (0.57± 0.02)	0.68± 0.013 (0.88± 0.015)
k_{on} ($M^{-1}.s^{-1}$)	2.91×10^5 (2.68×10^5)	1.67×10^5 (2.00×10^5)	1.31×10^5 (1.58×10^5)	0.90×10^5 (1.01×10^5)
k_{off} (s^{-1})	2.55×10^{-4} (2.51×10^{-4})	1.50×10^{-4} (1.32×10^{-4})	0.86×10^{-4} (0.90×10^{-4})	0.61×10^{-4} (0.89×10^{-4})

Values reported represent the global fit to the data using 1:1 binding model shown in (A - D). The experiments were done in duplicate, shown in parentheses.

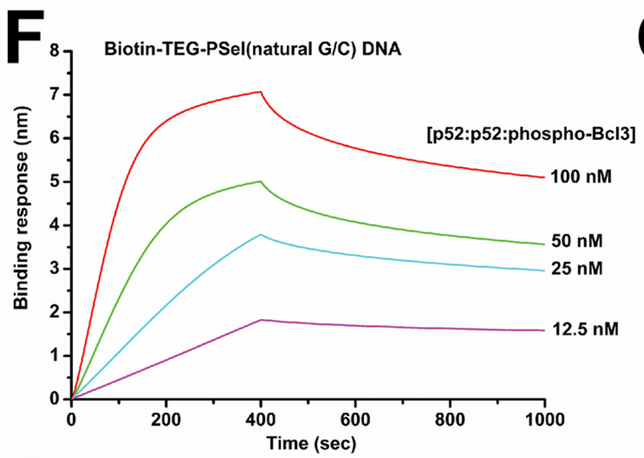

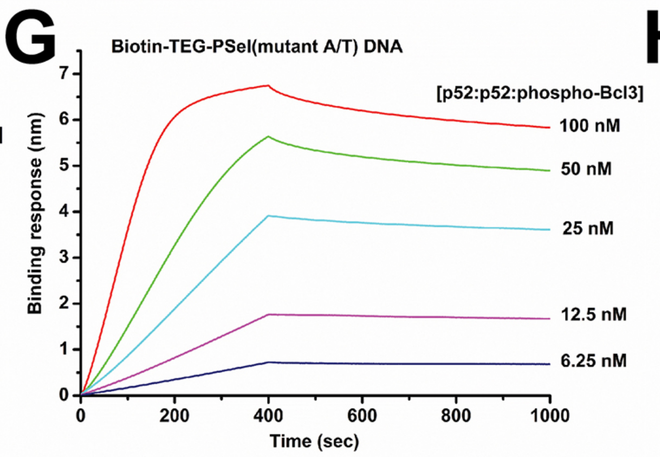

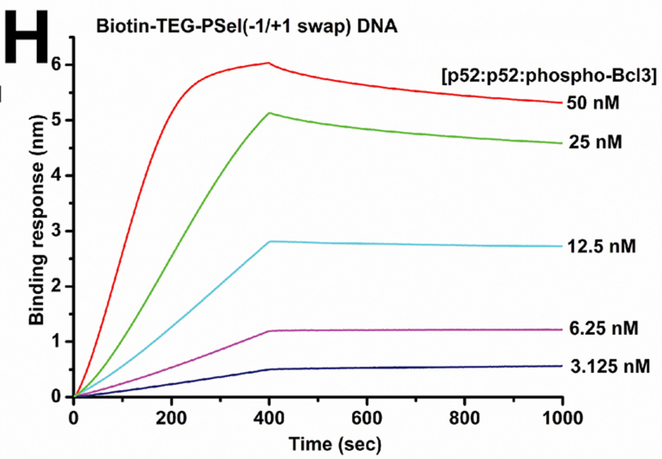

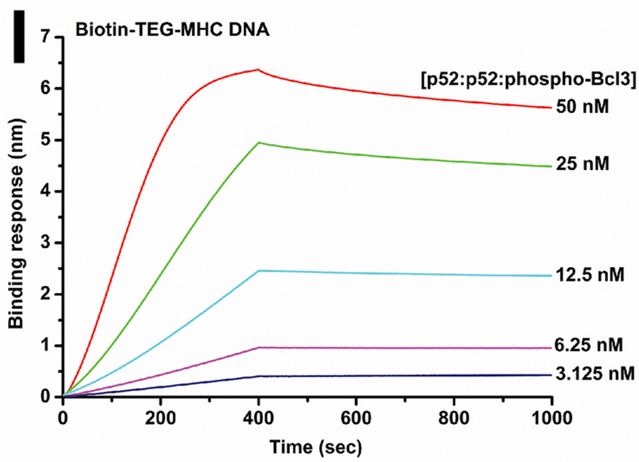

J **Kinetic analysis of p52:p52:Bcl3 complex binding to various κB DNAs by BLI**

	PSel(natual G/C-centric)	PSel(mutant A/T-centric)	PSel(-1/+1 swap)	MHC
K_d (nM)	5.21 ± 0.06 (5.43 ± 0.06)	2.93 ± 0.07 (2.91 ± 0.06)	1.62 ± 0.06 (1.64 ± 0.05)	2.62 ± 0.08 (3.31 ± 0.10)
k_{on} ($M^{-1}.s^{-1}$)	1.06×10^5 (1.0×10^5)	0.69×10^5 (0.71×10^5)	0.99×10^5 (1.08×10^5)	0.62×10^5 (0.52×10^5)
k_{off} (s^{-1})	5.52×10^{-4} (5.45×10^{-4})	2.01×10^{-4} (2.07×10^{-4})	1.61×10^{-4} (1.76×10^{-4})	1.63×10^{-4} (1.71×10^{-4})

Values reported represent the global fit to the data using 1:1 binding model shown in (F - I). The experiments were done in duplicate, shown in parentheses.

K

Fold Change / κB DNA		K_d Ratio = $\frac{K_d\ (X\ DNA)}{K_d\ (PSel\ G/C\text{-}centric)}$		k_{on} Ratio = $\frac{k_{on}(X\ DNA)}{k_{on}(PSel\ G/C\text{-}centric)}$		k_{off} Ratio = $\frac{k_{off}(X\ DNA)}{k_{off}(PSel\ G/C\text{-}centric)}$		RLU Ratio = $\frac{RLU\ (X\ DNA)}{RLU\ (PSel\ G/C\text{-}centric)}$
		(p52:p52)-DNA	(p52:p52:Bcl3)-DNA	(p52:p52)-DNA	(p52:p52:Bcl3)-DNA	(p52:p52)-DNA	(p52:p52:Bcl3)-DNA	(p52:p52:Bcl3)-DNA
PSel	natual G/C-centric	1.00	1.00	1.00	1.00	1.00	1.00	1.00
PSel	mutant A/T-centric	0.88	0.55	0.66	0.68	0.56	0.37	0.55
PSel	-1/+1 swap	0.68	0.31	0.52	1.01	0.35	0.31	0.09
MHC		0.86	0.56	0.34	0.55	0.30	0.30	0.26

Supplemental Information

Structures of NF-κB p52 homodimer-DNA complexes rationalize binding mechanisms and transcription activation

Vladimir A. Meshcheryakov, Wenfei Pan, Tianjie Li, Yi Wang, Gourisankar Ghosh, and Vivien Ya-Fan Wang

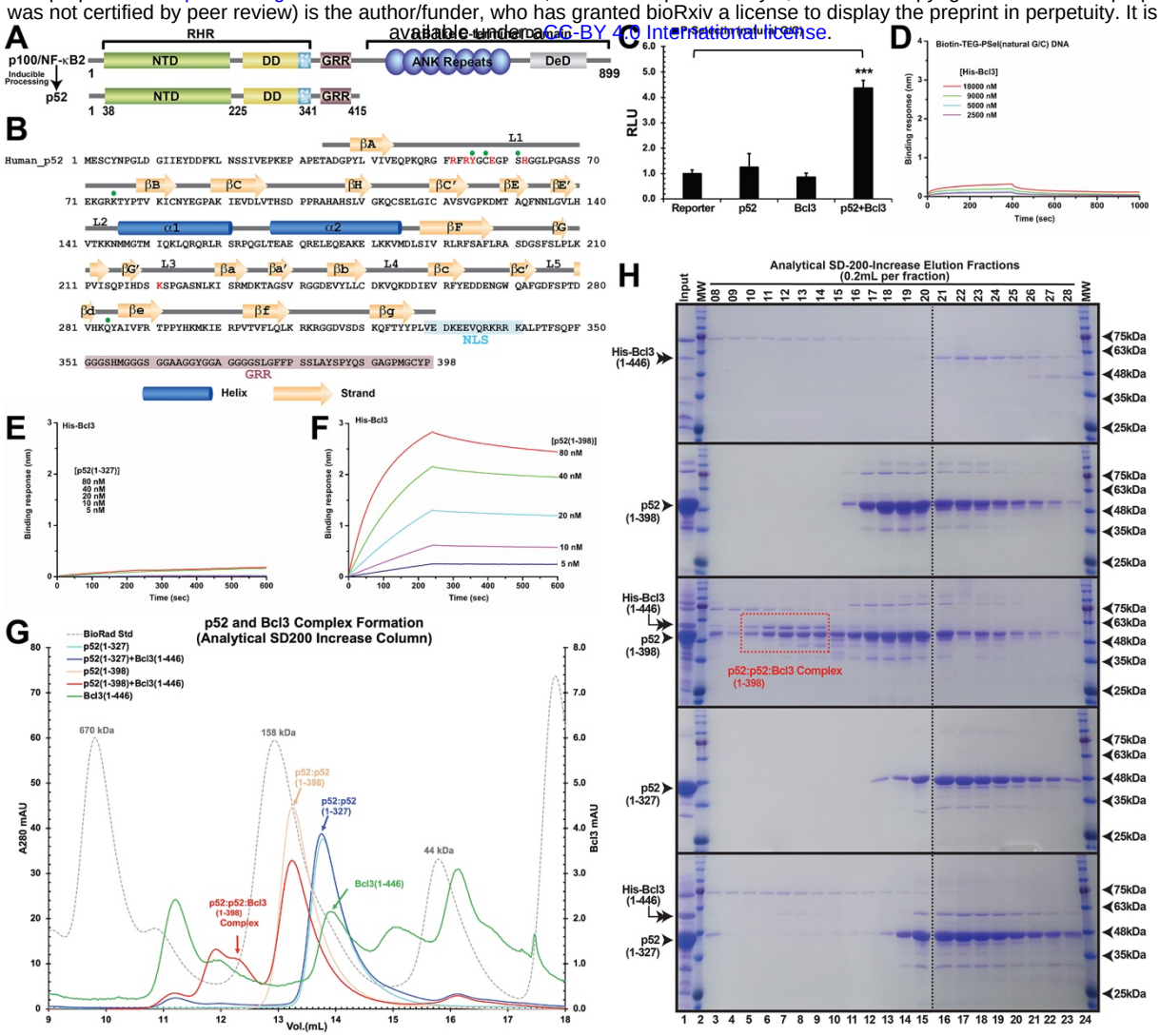

Figure S1. p52 and DNA crystallization. (A) Domain organization of the precursor protein p100/NF-κB2 and the processed p52. (B) Primary sequence of human p52 RHR. The secondary structures are mapped on top of the sequence. DNA base-specific contacting residues are denoted by red and backbone contacting residues are marked by green circle. NLS and GRR regions are highlighted in cyan and purple, respectively. (C) Co-expression of p52 and Bcl3, but not either one alone, activates the natural PSel luciferase reporter. The data were analyzed from three independent experiments performed in triplicate. RLU, relative luciferase unit. ***p<0.001 (t test). Error bars represent SD. (D) Biolayer interferometry (BLI) binding analysis of His-tagged-Bcl3 protein to immobilized biotin labeled natural PSel-κB DNA; the result indicated Bcl3 does not interact with κB DNA without p52 protein. (E-F) BLI binding analysis of (E) short p52:p52 (aa 1-327) and (F) long p52:p52 (aa 1-398) protein to immobilized His-tagged-Bcl3. The results showed only the long p52:p52 (aa 1-398) interacts with Bcl3 in (F). (G) Analytical Superdex-200-Increase size exclusion chromatography elution profile showing the long p52:p52 (aa 1-398) but not the short p52:p52 (aa 1-327) homodimer forms complex with Bcl3. (H) SDS-PAGE analysis indicating the p52:p52:Bcl3 complex formation in (G).

A

B

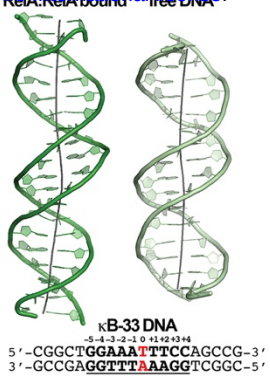

C

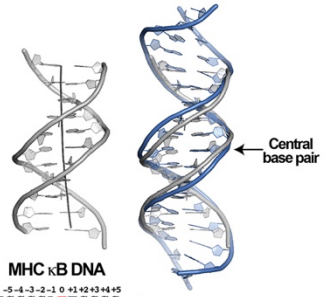

D

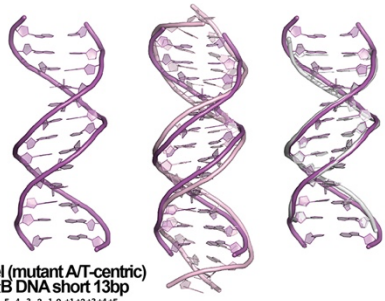

E

NF-κB Dimers	Protein Constructs (aa)	Electron Density (aa)	κB DNA Sequences	DNA Minor Groove Width (-1 to 0 position)	PDB
p50:p50	39-364	39-350	κB-55 -5 -4 -3 -2 -1 0 +1 +2 +3 +4 5′-TGGGAATTCCC -3′ 3′- CCCTTAAGGGT-5′	3.5 Å	1NFK
	2-364	43-353	-5 -4 -3 -2 -1 0 +1 +2 +3 +4 5′-AGATGGGGAATCCCCTAGA-3′ 3′-AGATCCCCTAAGGGGTAGA-5′	3.9 Å	1SVC
RelA:RelA	19-291	19-291	κB-33 -5 -4 -3 -2 -1 0 +1 +2 +3 +4 5′-CGGCTGGAAATTTCCAGCCG-3′ 3′-GCCGAGGTTTAAAGGTCGGC-5′	4.1 Å	1RAM
	19-304	19-291	E-selectin (mutant tandem sites) -4 -3 -2 -1 0 +1 +2 +3 +4 +5 5′-TAGCGGAAATTCCCGGGAATTTCCGCT -3′ 3′- TCGCCTTTAAGGGCCCTTAAAGGCGAT-5′ -5 -4 -3 -2 -1 0 +1 +2 +3 +4	3.8 Å; 3.4 Å	5U01
p50:RelA	p50 39-364 RelA 19-291	43-353 19-291	Ig-κB -5 -4 -3 -2 -1 0 +1 +2 +3 +4 5′-TGGGACTTTCC -3′ 3′- CCCCTGAAAGGA-5′	3.9 Å	1VKX
	p50 39-350 RelA 19-291	39-350 19-291	Ig/HIV-2 -5 -4 -3 -2 -1 0 +1 +2 +3 +4 5′-TGGGACTTTCCT-3′ 3′-ACCCTGAAAGGA-5′	3.9 Å	1LE9
	p50 39-350 RelA 19-291	43-350 19-291	IFNβ -5 -4 -3 -2 -1 0 +1 +2 +3 +4 5′-TGGGAAATTCCT -3′ 3′- CCCTTTAAGGAA-5′	3.4 Å	1LE5
	p50 39-350 RelA 19-291	43-350 19-291	IFNβ -5 -4 -3 -2 -1 0 +1 +2 +3 +4 5′-AGTGGGAAATTCCTCTG-3′ 3′-TCACCCTTTAAGGAGAC-5′	3.6 Å	2I9T
c-Rel:c-Rel	7-281	7-281	IL-2 -4 -3 -2 -1 0 +1 +2 +3 +4 5′-GGGTTTAAAGAAATTCCAGA-3′ 3′-CCCAAATTTCTTTAAGGTCT-5′	3.6 Å	1GJI
p52:p52	35-329	37-327	MHC -5 -4 -3 -2 -1 0 +1 +2 +3 +4 +5 5′-TTGGGGATTCCCC -3′ 3′- ACCCCTAAGGGGT-5′	3.8 Å	1A3Q
	1-398	34-329	P-selectin (natural G/C-centric) -5 -4 -3 -2 -1 0 +1 +2 +3 +4 +5 5′-GAAGGGGGTGACCCCTTG-3′ 3′-CTTCCCCCACTGGGGAAC-5′ (this study)	7.7 Å	7CLI
	1-398	34-329	P-selectin (mutant A/T-centric) -5 -4 -3 -2 -1 0 +1 +2 +3 +4 +5 5′-GAAGGGGGTAACCCCTTG-3′ 3′-CTTCCCCCATTGGGGAAC-5′ (this study)	7.4 Å	7VUQ
	1-398	34-327	P-selectin (-1/+1 swap) -5 -4 -3 -2 -1 0 +1 +2 +3 +4 +5 5′-GAAGGGGGAGTCCCCTTG-3′ 3′-CTTCCCCCTCAGGGGAAC-5′ (this study)	7.5 Å	7VUP
	1-327	33-326	P-selectin (mutant A/T-centric) -5 -4 -3 -2 -1 0 +1 +2 +3 +4 +5 5′-GGGGGTAACCCCT-3′ 3′-CCCCCATTGGGGA-5′ (this study)	3.6 Å	7W7L
p50:RelB	p50 37-363 RelB 1-400	38-350 100-378	κB-55 -5 -4 -3 -2 -1 0 +1 +2 +3 +4 5′-CGGGAATTCCC -3′ 3′- CCCTTAAGGGC-5′	3.4 Å	2V2T
p52:RelB	p52 35-341 RelB 1-400	37-329 88-383	κB-55 -4 -3 -2 -1 0 +1 +2 +3 +4 +5 5′-CGGGAATTCCC -3′ 3′- CCCTTAAGGGC-5′	3.7 Å	3DO7

Figure S2. κB DNA conformations. (A) Structure of the κB-55 DNA in the (Left) p52:RelB-bound and (Right) free forms; free κB-55 DNA structure was obtained serendipitously where two κB-55 DNA molecules were found in the crystal, with one bound to the p52:RelB heterodimer and the other remained free (Fusco et al., 2009). (B) Structure of the 20bp κB-33 DNA in the (Left) RelA:RelA-bound (Chen et al., 1998) and (Right) free forms (Huang et al., 2005). (C) Structure of (Left) the 13bp MHC-κB DNA (Cramer et al., 1997) and (Right) overlay of natural G/C-centric PSel-κB DNA (in blue) with MHC-κB DNA (in gray), showing the widened minor groove in PSel-κB DNA. (D) Structure of (Left) short 13bp PSel (mutant A/T) κB DNA duplex in the co-crystal structure with short p52:p52 (aa 1-327) (in pink); overlay of 13bp PSel (mutant A/T) DNAs (in pink) with (Middle) the long 18bp PSel (mutant A/T) (in light pink), and (Right) the 13bp MHC-κB DNA (in gray). The DNA bps as observed in the co-crystal structures are shown in filled sticks. The view is onto the central minor groove. The nucleotide sequences used in co-crystallization are shown at the bottom, with κB DNA underlined and numbering scheme indicated above.(E) Table showing various nucleotide sequences used in co-crystallization with different NF-κB dimers The various NF-κB protein constructs used are also indicated. The κB DNAs are shown in bold, bases making contacts with NF-κB proteins are underlined, and the numbering scheme are indicated. The central bps are highlighted in red. The p52 protein construct and DNA sequences used in the current study are in blue. The MGW(s) from position −1 to 0 are listed. Geometrical parameters were calculated with Curves+ (Blanchet et al., 2011, Lavery et al., 2009).

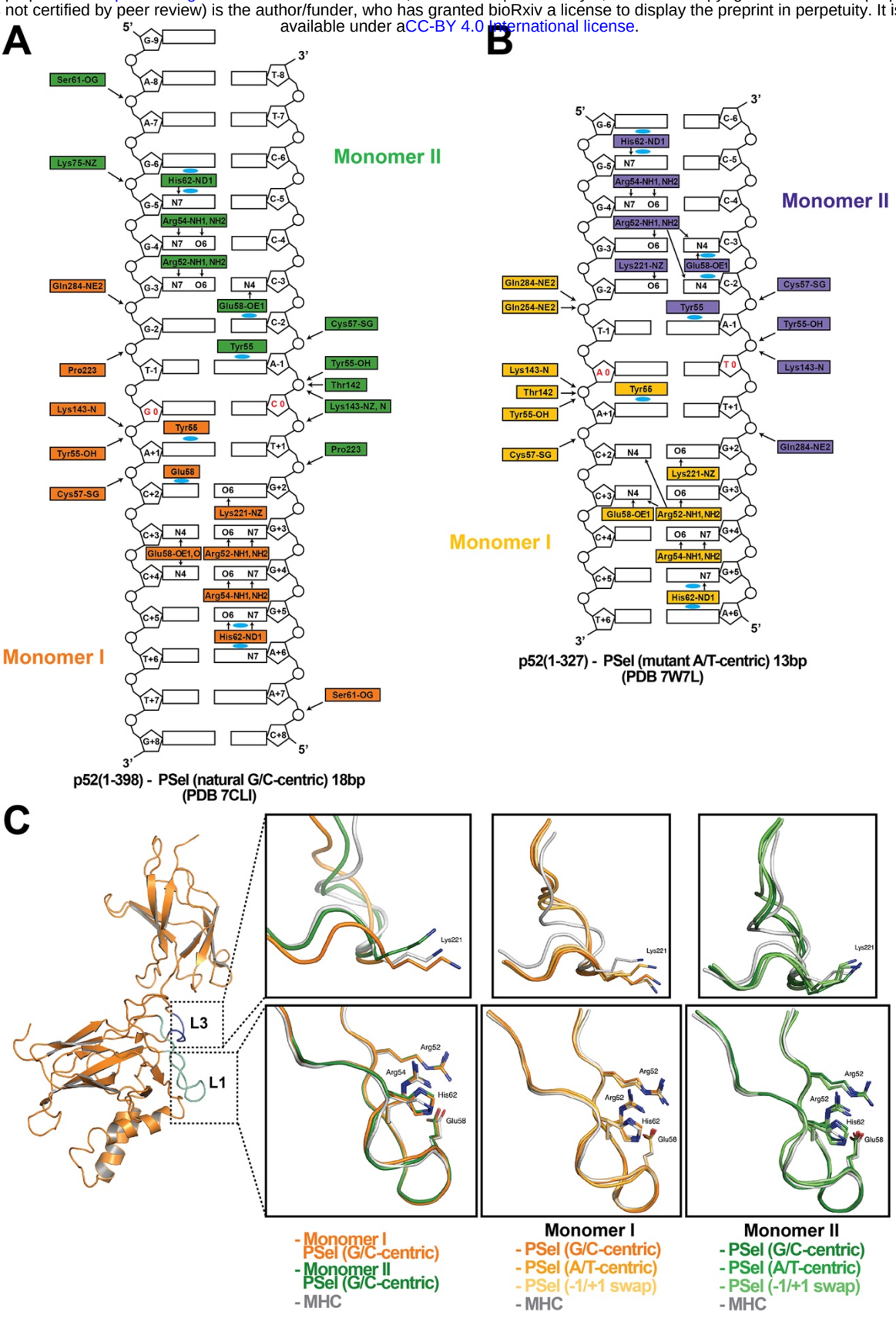

Figure S3. Asymmetric p52 monomers. (A-B) Schematic representation of the DNA contacts made by (A) the long p52:p52 (aa 1-398) with the 18bp natural PSel-κB DNA (PDB 7CLI); and (B) the short p52:p52 (aa 1-327) with the 13bp PSel(mutant A/T)-κB DNA (PDB 7W7L). Two colors indicate two different monomers within the complex. Arrows indicate H-bonds; cyan circles indicate van der Waals interactions. Arg52(s) from both monomers make cross-strand DNA contacts in (B) but not in (A). (C) Ribbon diagram of p52 monomer I, loops L1 (cyan) and L3 (blue) are highlighted. Residues in these two loops make base-specific contacts with DNA. The zoom-in views show overlays of loops L1 and L3 in (p52:p52)-PSel and (p52:p52)-MHC complexes with indicated colors.

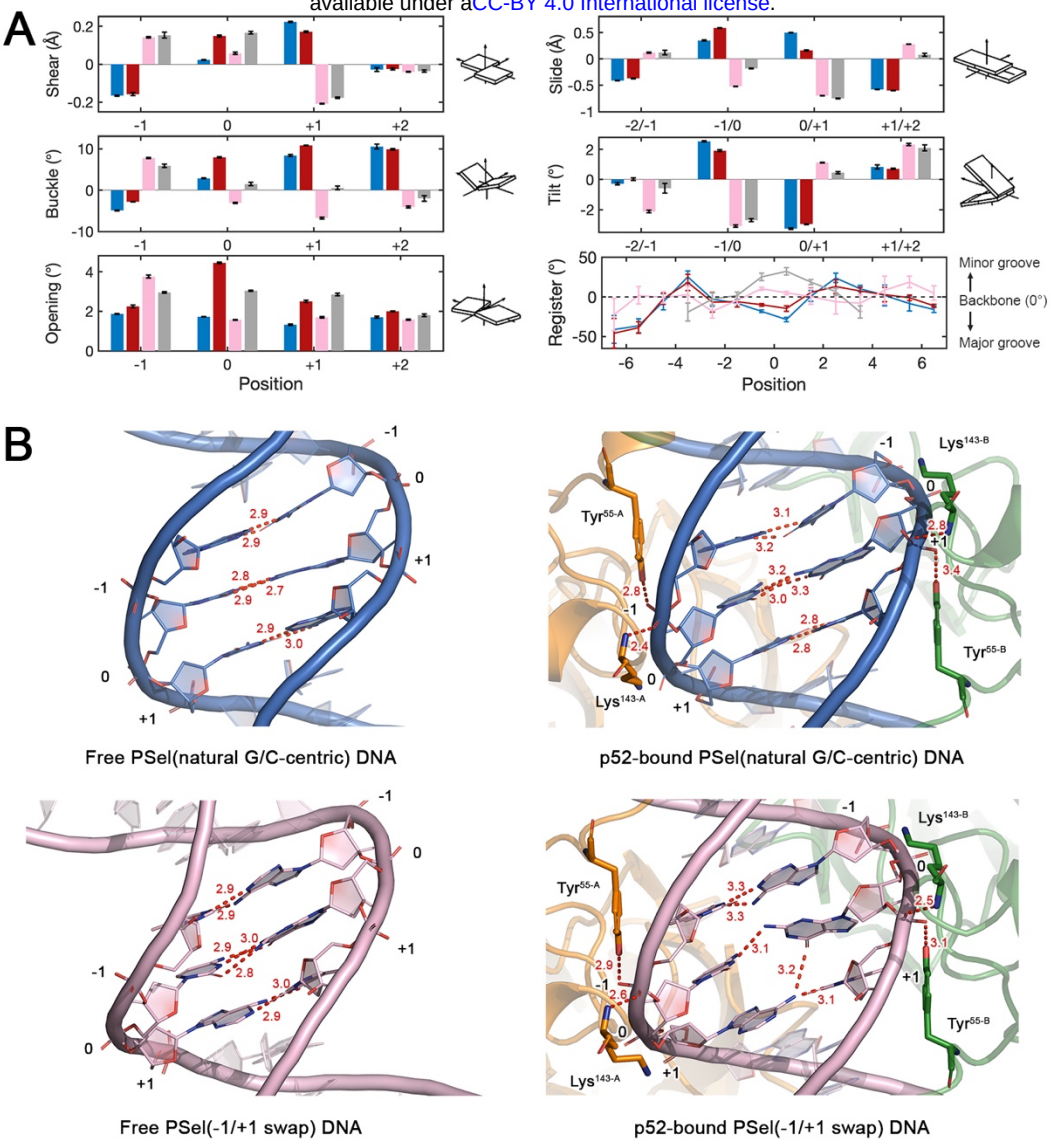

Figure S4. Free DNA simulations. (A) Geometric parameters at −1 to +2 positions revealed in the MD simulations. The swap of T and A at ±1 positions causes an opposite shear and buckle of the nucleotide, which leads to a slide and tilt of the central bps towards the minor groove in −1/+1 swap DNA and therefore narrows the central minor grooves; A:T has a larger shear and opening at the 0 position compared to G:C which might have led to the decrease in minor groove width at +1 position. Geometrical parameters and the helical axes were calculated with Curves+ (Blanchet et al., 2011, Lavery et al., 2009). Corresponding schematic images of each parameter are viewed from the minor groove and shown in the positive sense. Error bars represent standard error of the mean (SEM) computed from the five replica simulations of a given system.(B) Structure of natural G/C-centric and −1/+1 swap PSel-κB DNA in (Left) free forms from MD simulations and (Right) (p52:p52)-bound forms from crystal structures. Red dashed lines represent the intermolecular H-bonds formed at DNA's central part.

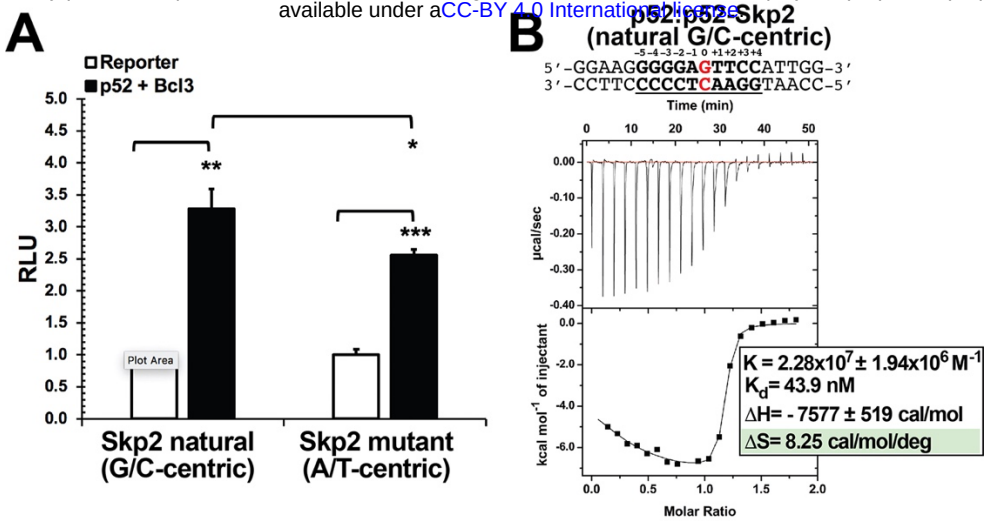

Figure S5. p52 interacts with Skp2-κB DNA. (A) The natural G/C-centric Skp2 luciferase reporter activity driven by co-expression of p52 and Bcl3; the corresponding A/T-centric mutant showed less transcription activity. The data were analyzed from three independent experiments performed in triplicate. RLU, relative luciferase unit. *p<0.05; **p<0.01; ***p<0.001 (t test). Error bars represent SD. (B) Calorimetric titration data showing the binding of recombinant p52:p52 homodimer with Skp2 G/C-centric κB DNA. The top panel of the ITC figures represent the binding isotherms; the bottom panel shows the integrated heat of the reaction and the line represents the best fit to the data according to a single-site binding model. The determined K_d, changes of enthalpy and entropy are shown on the bottom panel.

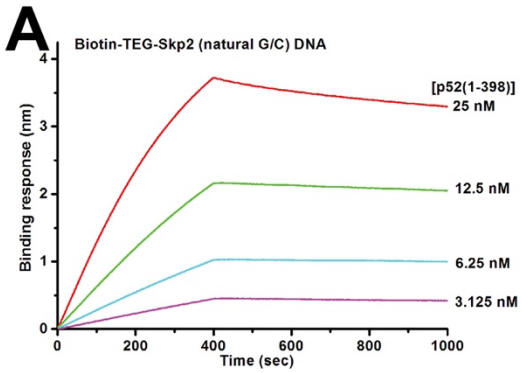

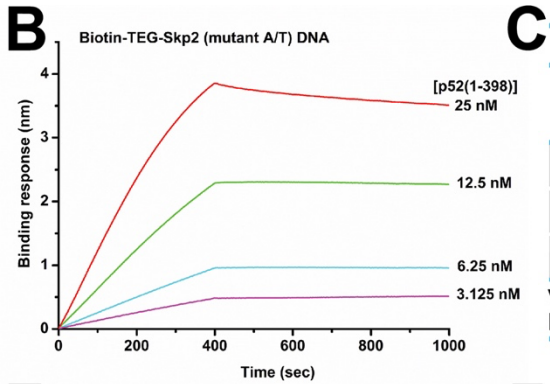

C

Kinetic analysis of p52:p52 homodimer binding to Skp2-κB DNA variants by BLI

	Skp2(natual G/C-centric)	Skp2(mutant A/T-centric)
K_d (nM)	1.91 ± 0.019 (2.24 ± 0.029)	0.981 ± 0.018 (0.982 ± 0.028)
k_{on} ($M^{-1}.s^{-1}$)	0.857 × 10^5 (0.65 × 10^5)	1.07 × 10^5 (0.91 × 10^5)
k_{off} (s^{-1})	1.63 × 10^{-4} (1.46 × 10^{-4})	1.05 × 10^{-4} (0.895 × 10^{-4})

Values reported represent the global fit to the data using 1:1 binding model shown in Fig. S6A - B. The experiments were done in duplicate, shown in parentheses.

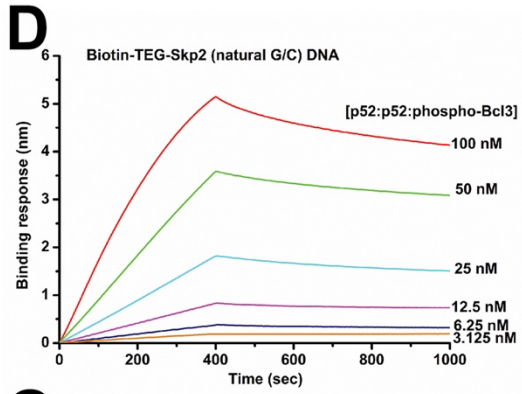

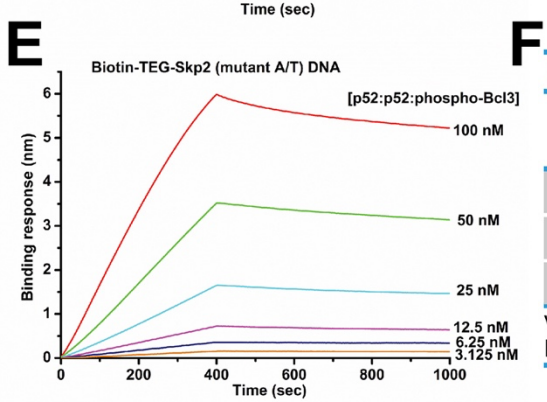

F

Kinetic analysis of p52:p52:Bcl3 complex binding to Skp2-κB DNA variants by BLI

	Skp2(natual G/C-centric)	Skp2(mutant A/T-centric)
K_d (nM)	13.8 ± 0.158 (10.2 ± 0.114)	15.6 ± 0.165 (21.3 ± 0.359)
k_{on} ($M^{-1}.s^{-1}$)	0.228 × 10^5 (0.284 × 10^5)	0.147 × 10^5 (0.0999 × 10^5)
k_{off} (s^{-1})	3.14 × 10^{-4} (2.90 × 10^{-4})	2.29 × 10^{-4} (2.13 × 10^{-4})

Values reported represent the global fit to the data using 1:1 binding model shown in Fig. S6D - E. The experiments were done in duplicate, shown in parentheses.

G

Fold Change / κB DNA		K_d Ratio = $\frac{K_d\text{ (Skp2 A/T-centric)}}{K_d\text{ (Skp2 G/C-centric)}}$		k_{on} Ratio = $\frac{k_{on}\text{(Skp2 A/T-centric)}}{k_{on}\text{(Skp2 G/C-centric)}}$		k_{off} Ratio = $\frac{k_{off}\text{(Skp2 A/T-centric)}}{k_{off}\text{(Skp2 G/C-centric)}}$		RLU Ratio = $\frac{\text{RLU (Skp2 A/T-centric)}}{\text{RLU (Skp2 G/C-centric)}}$
		(p52:p52)-DNA	(p52:p52:Bcl3)-DNA	(p52:p52)-DNA	(p52:p52:Bcl3)-DNA	(p52:p52)-DNA	(p52:p52:Bcl3)-DNA	(p52:p52:Bcl3)-DNA
Skp2	natual G/C-centric	1.00	1.00	1.00	1.00	1.00	1.00	1.00
	mutant A/T-centric	0.47	1.54	1.31	0.48	0.63	0.73	0.78

Figure S6. p52 and Skp2-κB DNA binding kinetics. (A-B) BLI binding analysis of p52:p52 (aa 1-398) homodimer to immobilized biotin labeled (A) Skp2 natural G/C-centric and (B) mutant A/T-centric DNAs. Each experiment was done in duplicate and one representative set of curves is shown. (C) Table showing the kinetic analysis in (A) and (B). (D-E) BLI binding analysis of p52:p52:Bcl3 complex to immobilized biotin labeled (D) Skp2 natural G/C-centric and (E) mutant A/T-centric DNAs. Each experiment was done in duplicate and one representative set of curves is shown. (F) Table showing the kinetic analysis in (D) and (E). (G) Table summarizing the fold change of K_d, k_{on} and k_{off} with respect to the more transcriptionally active G/C-centric Skp2-κB DNA. The average values of the duplicated kinetics data in (A-F) and the relative reporter activities in RLU from Fig. S5A were used for ratio calculations. The numbers for the greater reporter active G/C-centric Skp2 DNAs are shown in blue.

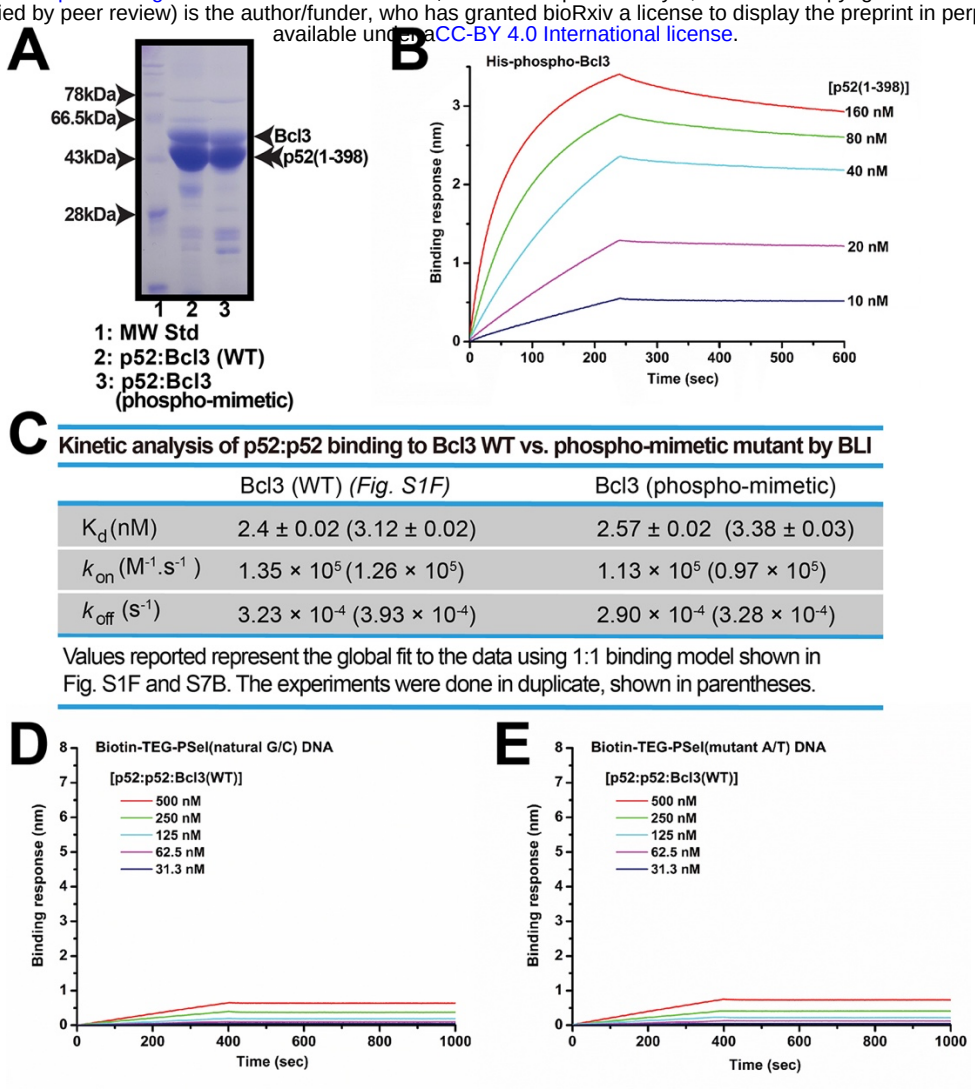

Figure S7. Recombinant phospho-mimetic Bcl3 forms a ternary complex with p52 and κB DNA. (A) SDS-PAGE analysis showing the p52:p52:Bcl3 WT vs. phospho-mimetic mutant complexes with similar purity. (B) BLI analysis of p52 to immobilized His-tagged-Bcl3 phospho-mimetic mutant protein. (C) Table showing the kinetic analysis in Figures S1F and S7B, suggesting p52:p52 homodimer interacts with WT and phospho-mimetic Bcl3 with similar affinity and kinetics. (D-E) BLI analysis of p52:p52:Bcl3 (WT) complex to immobilized PSel (D) natural G/C-centric and (E) mutant A/T-centric DNAs. The WT complex does not interact with either DNAs. Each experiment was done in duplicate and one representative set of curves is shown.

Table S1. Summary of protein-DNA contacts.

	p52:p52-PSel(natural G/C-centric)_18bp (PDB 7CLI) *(this study)*						p52:p52-PSel(mutant A/T-centric)_18bp (PDB 7VUQ) *(this study)*						p52:p52-PSel(-1/+1 SWAP)_18bp (PDB 7VUP) *(this study)*					
	p52 Monomer Ⅰ			p52 MonomerⅡ			p52 Monomer Ⅰ			p52 MonomerⅡ			p52 Monomer Ⅰ			p52 MonomerⅡ		
	DNA	Protein	Distance (Å)	DNA	Protein	Distance (Å)	DNA	Protein	Distance (Å)	DNA	Protein	Distance (Å)	DNA	Protein	Distance (Å)	DNA	Protein	Distance (Å)
Backbone	A(+7) OP2	Ser61 OG	2.79	A(-7) OP2	Ser61 OG	3.13	A(+7) OP2	Ser61 OG	2.66	A(-7) OP2	Ser61 OG	3.13	A(+7) OP2	Ser61 OG	2.75	A(-7) OP2	Ser61 OG	2.61
	A(+6) N7	Ser61 O	x(3.49)	G(-6) N7	Ser61 O	x(3.85)	A(+6) N7	Ser61 O	x(3.57)	G(-6) N7	Ser61 O	3.08	A(+6) N7	Ser61 O	3.28	G(-6) N7	Ser61 O	3.20
	x	x	x	G(-5) OP1	Lys75 NZ	3.13	x	x	x	G(-5) OP1	Lys75 NZ	x(5.79)	x	x	x	G(-5) OP1	Lys75 NZ	x(4.78)
				G(-5) OP2		x(3.70)				G(-5) OP2		x(6.14)				G(-5) OP2		x(5.40)
Base contact	G(+5) O6	His62 ND1	3.26	G(-5) O6	His62 ND1	x(3.57)	G(+5) O6	His62 ND1	3.12	G(-5) O6	His62 ND1	x(3.67)	G(+5) O6	His62 ND1	x(3.43)	G(-5) O6	His62 ND1	x(3.62)
	G(+5) N7		2.93	G(-5) N7		2.80	G(+5) N7		2.88	G(-5) N7		3.09	G(+5) N7		3.10	G(-5) N7		x(3.52)
	G(+4) O6	Arg54 NH1	3.08	G(-4) O6	Arg54 NH1	3.19	G(+4) O6	Arg54 NH1	3.16	G(-4) O6	Arg54 NH1	3.36	G(+4) O6	Arg54 NH1	3.03	G(-4) O6	Arg54 NH1	2.76
		Arg54 NH2	x(4.48)		Arg54 NH2	x(4.54)		Arg54 NH2	x(4.65)		Arg54 NH2	x(4.50)		Arg54 NH2	x(4.18)		Arg54 NH2	x(3.88)
	G(+4) N7	Arg54 NH1	x(3.66)	G(-4) N7	Arg54 NH1	x(3.63)	G(+4) N7	Arg54 NH1	x(3.45)	G(-4) N7	Arg54 NH1	x(3.84)	G(+4) N7	Arg54 NH1	x(3.65)	G(-4) N7	Arg54 NH1	x(3.91)
		Arg54 NH2	3.27		Arg54 NH2	3.22		Arg54 NH2	3.08		Arg54 NH2	3.27		Arg54 NH2	2.92		Arg54 NH2	3.18
		Arg52 NH1	x(3.92)		Arg52 NH1	x(4.53)		Arg52 NH1	x(4.34)		Arg52 NH1	x(3.80)		Arg52 NH1	x(3.72)		Arg52 NH1	2.94
	G(+3) O6	Arg52 NH1	x(4.14)	G(-3) O6	Arg52 NH1	2.76	G(+3) O6	Arg52 NH1	3.27	G(-3) O6	Arg52 NH1	x(3.86)	G(+3) O6	Arg52 NH1	x(3.73)	G(-3) O6	Arg52 NH1	x(3.96)
		Arg52 NH2	3.19		Arg52 NH2	x(3.71)		Arg52 NH2	2.41		Arg52 NH2	2.74		Arg52 NH2	2.83		Arg52 NH2	3.15
	G(+3) N7	Arg52 NH1	3.24	G(-3) N7	Arg52 NH1	x(4.30)	G(+3) N7	Arg52 NH1	3.37	G(-3) N7	Arg52 NH1	x(3.48)	G(+3) N7	Arg52 NH1	3.17	G(-3) N7	Arg52 NH1	x(3.71)
		Arg52 NH2	x(4.19)		Arg52 NH2	3.26		Arg52 NH2	x(4.44)		Arg52 NH2	x(4.26)		Arg52 NH2	x(4.14)		Arg52 NH2	x(4.45)
	G(+2) O6	Lys221 NZ	2.63	G(-2) O6	Lys221 NZ	x(4.46)	G(+2) O6	Lys221 NZ	x(3.53)	G(-2) O6	Lys221 NZ	x(5.36)	G(+2) O6	Lys221 NZ	2.13	G(-2) O6	Lys221 NZ	x(5.29)
	x	x	x	x	x	x	x	x	x	x	x	x	x	x	x	x	x	x
Backbone	G(-2) OP1	Gln284 NE2	2.79	x	x	x	G(-2) OP1	Gln284 NE2	2.73	x	x	x	G(-2) OP1	Gln284 NE2	2.44	G(+2) OP1	Gln284 NE2	2.54
	x	x	x	x	x	x	x	x	x	x	x	x	x	x	x	x	x	x
	T(-1) OP1	x	x	x	x	x	T(-1) OP1	x	x	x	x	x	A(-1) OP1	x	x	A(+1) OP1	x	x
		Pro223 CB	3.15	T(+1) OP1	Pro223 CB	3.28		Pro223 CB	3.35	T(+1) OP1	Pro223 CB	x(3.49)		Pro223 CB	3.29		Pro223 CB	x(3.51)
	G(0) OP1	Pro223 CD	x(3.75)	C(0) OP1	x	x	A(0) OP1	Pro223 CD	x(4.31)	T(0) OP1	x	x	G(0) OP1	Pro223 CD	x(3.82)	C(0) OP1	x	x
		Pro223 CG	x(3.77)		x	x		Pro223 CG	x(4.47)		x	x		Pro223 CG	x(3.89)		x	x
		Lys143 NZ	x(5.33)		Lys143 NZ	3.38		Lys143 NZ	x(4.79)		Lys143 NZ	x(5.27)		Lys143 NZ	x(5.33)		Lys143 NZ	x(5.11)
	A(+1) OP2	Tyr55 OH	3.40	A(-1)OP2	Tyr55 OH	2.77	A(+1) OP2	Tyr55 OH	2.71	A(-1)OP2	Tyr55 OH	2.55	T(+1) OP2	Tyr55 OH	3.05	T(-1)OP2	Tyr55 OH	2.94
	A(+1) OP1	Thr142 C	x(4.14)	A(-1) OP1	Thr142 C	3.27	A(+1) OP1	Thr142 C	3.28	A(-1) OP1	Thr142 C	x(3.58)	T(+1) OP1	Thr142 C	3.33	T(-1) OP1	Thr142 C	x(3.42)
		Thr142 CA	x(3.74)		Thr142 CA	3.20		Thr142 CA	3.12		Thr142 CA	3.39		Thr142 CA	3.32		Thr142 CA	3.35
		Lys143 N	2.79	A(-1) OP1	Lys143 N	2.45		Lys143 N	2.57		Lys143 N	2.84		Lys143 N	2.47		Lys143 N	2.59
	C(+2) OP2	Cys57 SG	x(3.52)	C(-2) OP2	Cys57 SG	x(3.64)	C(+2) OP2	Cys57 SG	x(3.72)	C(-2) OP2	Cys57 SG	x(3.57)	C(+2) OP2	Cys57 SG	x(3.80)	C(-2) OP2	Cys57 SG	x(3.59)
	C(+2) O5'		x(3.41)	C(-2) O5'		3.36	C(+2) O5'		3.08	C(-2) O5'		3.09	C(+2) O5'		3.37	C(-2) O5'		3.35
Base contact	C(+2) N4	x	x	C(-2) N4	x	x	C(+2) N4	x	x	C(-2) N4	x	x	C(+2) N4	x	x	C(-2) N4	x	x
		Arg52 NH2	x(3.57)		Arg52 NH2	x(5.40)		Arg52 NH2	x(3.56)		Arg52 NH2	x(3.72)		Arg52 NH2	x(3.47)		Arg52 NH2	3.27
	C(+3) N4	Arg52 NH2	x(3.59)	C(-3) N4	Arg52 NH1	x(3.48)	C(+3) N4	Arg52 NH2	x(3.70)	C(-3) N4	Arg52 NH2	x(3.67)	C(+3) N4	Arg52 NH2	x(4.19)	C(-3) N4	Arg52 NH2	x(3.69)
		Glu58 OE1	3.04		Glu58 OE1	3.23		Glu58 OE1	2.91		Glu58 OE1	3.06		Glu58 OE1	x(3.43)		Glu58 OE1	x(3.64)
	C(+4) N4	Glu58 O	3.32	C(-4) N4	Glu58 O	x(4.47)	C(+4) N4	Glu58 O	x(3.73)	C(-4) N4	Glu58 O	x(3.77)	C(+4) N4	Glu58 O	x(4.10)	C(-4) N4	Glu58 O	x(5.98)

	p52:p52-PSel(mutant A/T-centric)_13bp (PDB 7W7L) *(this study)*						p52:p52-MHC (PDB 1A3Q)						p50:RelA-IFNβ (PDB 1LE5)					
	p52 Monomer Ⅰ			p52 MonomerⅡ			p52 Monomer Ⅰ			p52 MonomerⅡ			RelA subunit			p50 subunit		
	DNA	Protein	Distance (Å)	DNA	Protein	Distance (Å)	DNA	Protein	Distance (Å)	DNA	Protein	Distance (Å)	DNA	Protein	Distance (Å)	DNA	Protein	Distance (Å)
Backbone																		
Base contact	G(+5) O6	His62 ND1	x(3.53)	G(-5) O6	His62 ND1	x(3.44)	G(+5) O6	His62 ND1	3.40	x	x	x				G(-5) O6	His64 ND1	2.70
	G(+5) N7		2.76	G(-5) N7		2.67	G(+5) N7		2.82	x		x				G(-5) N7		x(3.65)
	G(+4) O6	Arg54 NH1	2.81	G(-4) O6	Arg54 NH1	2.69	G(+4) O6	Arg54 NH1	3.14	G(-4) O6	Arg54 NH1	2.99	G(+4) O6	Arg35 NH1	x(3.72)	G(-4) O6	Arg56 NH1	x(5.08)
		Arg54 NH2	x(3.87)		Arg54 NH2	x(3.76)		Arg54 NH2	x(4.23)		Arg54 NH2	x(4.18)		Arg35 NH2	x		Arg56 NH2	x(5.53)
	G(+4) N7	Arg54 NH1	x(3.72)	G(-4) N7	Arg54 NH1	x(3.67)	G(+4) N7	Arg54 NH1	x(3.58)	G(-4) N7	Arg54 NH1	x(3.67)	G(+4) N7	Arg35 NH1	x(5.10)	G(-4) N7	Arg56 NH2	x(5.44)
		Arg54 NH2	2.74		Arg54 NH2	2.68		Arg54 NH2	3.04		Arg54 NH2	3.03		Arg35 NH2	x		Arg56 NH2	x(4.89)
		Arg52 NH1	x(4.68)		Arg52 NH1	x(4.74)		Arg52 NH1	3.16		Arg52 NH1	2.85		Arg33 NH1	3.38		Arg54 NH1	x(4.26)
	G(+3) O6	Arg52 NH1	2.69	G(-3) O6	Arg52 NH1	2.72	G(+3) O6	Arg52 NH1	2.89	G(-3) O6	Arg52 NH1	x(3.79)	G(+3) O6	Arg33 NH1	x(4.04)	G(-3) O6	Arg54 NH1	2.80
		Arg52 NH2	3.06		Arg52 NH2	3.26		Arg52 NH2	2.82		Arg52 NH2	3.29		Arg33 NH2	2.99		Arg54 NH2	x(4.05)
	G(+3) N7	Arg52 NH1	x(4.96)	G(-3) N7	Arg52 NH1	x(4.78)	G(+3) N7	Arg52 NH1	x(3.65)	G(-3) N7	Arg52 NH1	x(4.07)	G(+3) N7	Arg33 NH1	2.83	G(-3) N7	Arg54 NH1	x(4.05)
		Arg52 NH2	x(3.72)		Arg52 NH2	x(3.61)		Arg52 NH2	x(4.93)		Arg52 NH2	x(4.78)		Arg33 NH2	3.55		Arg54 NH2	x(5.51)
	G(+2) O6	Lys221 NZ	2.64	G(-2) O6	Lys221 NZ	2.87	G(+2) O6	Lys221 NZ	2.84	G(-2) O6	Lys221 NZ	2.76	x	x	x	A(-2) N6	Arg54 NH2	2.95
	x	x	x	x	x	x	x	x	x	x	x	x	x	x	x	T(-1) O4	Lys241 NZ	x(3.47)
Backbone	G(-2) OP1	Gln284 NE2	x(6.41)	x	x	x	x	x	x	x	x	x						
	T(-1) OP2	Gln284 NE2	3.30	T(+1) OP2	Gln284 NE2	2.83	A(-1) OP1	Gln254 NE2	x(4.21)	A(+1) OP1	Gln254 NE2	2.76				A(+1) OP1	Gln274 NE2	x(3.78)
								Gln284 NE2	x(3.47)		Gln284 NE2	3.30						
	T(-1) OP1	Gln254 NE2	3.23	T(+1) OP1	Gln254 NE2	x(3.46)	A(-1) OP2	Gln284 NE2	3.28	A(+1) OP2	Gln284 NE2	3.33				A(+1) OP2	Gln306 NE2	x(3.78)
		Pro223 CB	x(3.83)		Pro223 CB	x(3.85)		Pro223 CB	3.30		Pro223 CB	x(3.60)					Gln306 OE1	2.88
								Pro223 CG	3.39		Pro223 CG	3.39						
	A(0) OP2	Pro223 CD	x(3.89)	T(0) OP1	Pro223 CD	x(3.60)	A(0) OP2	Pro223 CD	x(3.44)	T(0) OP2	Pro223 CD	x(3.47)						
		Pro223 CG	x(4.69)		Pro223 CG	x(4.42)												
		Lys143 NZ	x(7.64)		Lys143 NZ	x(3.47)												
	A(+1) OP2	Tyr55 OH	2.54	A(-1)OP2	Tyr55 OH	2.66	T(+1) OP2	Tyr55 OH	2.66	T(-1) OP2	Tyr55-OH	2.67	T(+1) OP2	Tyr 36 OH	2.31	T(-1) OP2	Tyr 57 OH	x(4.56)
	A(+1) OP1	Thr142 C	x(3.44)	A(-1) OP1	Thr142 C	x(3.67)	T(+1) OP1	Thr142 CA	3.50	T(-1) OP1	Thr142 CA	x(3.82)	T(+1) OP1	Lys123 N	x(3.65)	T(-1) OP1	Lys144 N	x(3.91)
		Thr142 CA	3.20		Thr142 CA	x(3.41)		Lys143 N	2.83		Lys143 N	3.01						
		Lys143 N	2.76		Lys143 N	2.97												
	C(+2) OP2	Cys57 SG	x(3.43)	C(-2) OP2	Cys57 SG	3.04	C(+2) OP2	Cys57 SG	x(3.46)	C(-2) OP2	Cys57 SG	x(3.54)				T(-2) OP2	Cys59 N	2.98
	C(+2) O5'		3.23	C(-2) O5'		3.15	C(+2) O5'		3.38	C(-2) O5'		3.29						
Base contact	C(+2) N4	x	x	C(-2) N4	x	x	C(+2) N4	x	x	C(-2) N4	x	x	T(+2) O4	Arg187 NH2	2.57	T(-2) O4	x	x
		Arg52 NH1	3.26		Arg52 NH1	3.23		Arg52 NH2	2.92		Arg52 NH2	3.02		Arg35 NH2	x(3.53)		Arg54 NH2	2.32
	C(+3) N4	Arg52 NH1	3.09	C(-3) N4	Arg52 NH1	3.26	C(+3) N4	Arg52 NH2	3.39	C(-3) N4	Arg52 NH2	x(3.78)	C(+3) N4	Arg35 NH1	3.28	C(-3) N4	Arg54 NH1	x(4.42)
		Glu58 OE1	2.90		Glu58 OE1	3.05		Glu58 OE1	3.01		Glu58 OE1	2.60		Glu39 OE1	2.80		Glu60 OE1	x(3.98)
	C(+4) N4	Glu58 O	x(3.63)	C(-4) N4	Glu58 O	x(3.42)	C(+4) N4	Glu58 O	x(3.82)	x	x	x	x	x	x			

Blue: Base specific contacts

Black: Phosphate backbone contacts

x(number): No H-bonds (distance more than 3.40Å), numbers in parentheses are distances shown as references

Yellow highlight: Most significantly different regions in p52-P-Selectin structure vs. previous known NF-κB-DNA structures

References

BLANCHET, C., PASI, M., ZAKRZEWSKA, K. & LAVERY, R. 2011. CURVES+ web server for analyzing and visualizing the helical, backbone and groove parameters of nucleic acid structures. *Nucleic Acids Res,* 39**,** W68-73.

CHEN, Y. Q., GHOSH, S. & GHOSH, G. 1998. A novel DNA recognition mode by the NF-kappa B p65 homodimer. *Nat Struct Biol,* 5**,** 67-73.

CRAMER, P., LARSON, C. J., VERDINE, G. L. & MULLER, C. W. 1997. Structure of the human NF-kappaB p52 homodimer-DNA complex at 2.1 A resolution. *EMBO J,* 16**,** 7078-90.

FUSCO, A. J., HUANG, D. B., MILLER, D., WANG, V. Y., VU, D. & GHOSH, G. 2009. NF-kappaB p52:RelB heterodimer recognizes two classes of kappaB sites with two distinct modes. *EMBO Rep,* 10**,** 152-9.

HUANG, D. B., PHELPS, C. B., FUSCO, A. J. & GHOSH, G. 2005. Crystal structure of a free kappaB DNA: insights into DNA recognition by transcription factor NF-kappaB. *J Mol Biol,* 346**,** 147-60.

LAVERY, R., MOAKHER, M., MADDOCKS, J. H., PETKEVICIUTE, D. & ZAKRZEWSKA, K. 2009. Conformational analysis of nucleic acids revisited: Curves+. *Nucleic Acids Res,* 37**,** 5917-29.